Received: 18 December 2015 | Revised: 17 October 2016 | Accepted: 6 November 2016

DOI 10.1002/cne.24154

RESEARCH ARTICLE

WILEY The Journal of Comparative Neurology

Inflammation of peripheral tissues and injury to peripheral nerves induce differing effects in the expression of the calcium-sensitive N-arachydonoylethanolamine-synthesizing enzyme and related molecules in rat primary sensory neurons

João Sousa-Valente[1] | Angelika Varga[1,2] | Jose Vicente Torres-Perez[1] | Agnes Jenes[1,2] | John Wahba[1] | Ken Mackie[3] | Benjamin Cravatt[4] | Natsuo Ueda[5] | Kazuhito Tsuboi[5] | Peter Santha[6] | Gabor Jancso[6] | Hiren Tailor[1] | António Avelino[7,8] | Istvan Nagy[1]

[1]Section of Anaesthetics, Pain Medicine and Intensive Care, Department of Surgery and Cancer, Imperial College London, Chelsea and Westminster Hospital, London SW10 9NH, United Kingdom

[2]Department of Physiology, University of Debrecen, Medical and Health Science Center, Debrecen H-4012, Hungary

[3]Department of Psychological and Brain Sciences, Gill Center for Biomedical Sciences, Indiana University, Bloomington, Indiana 47405

[4]The Skaggs Institute for Chemical Biology and Department of Chemical Physiology, The Scripps Research Institute, La Jolla, California 92037

[5]Department of Biochemistry, Kagawa University School of Medicine, Miki, Kagawa 761-0793, Japan

[6]Department of Physiology, University of Szeged, 6720 Szeged, Hungary

[7]Departamento de Biologia Experimental, Faculdade de Medicina do Porto, 4200-450 Porto, Portugal

[8]I3S Instituto de Investigação e Inovação em Saúde, IBMC Instituto de Biologia Molecular e Celular, 4200-135 Porto, Portugal

Correspondence
Istvan Nagy, Section of Anaesthetics, Pain Medicine and Intensive Care, Department of Surgery and Cancer, Imperial College London, Chelsea and Westminster Hospital, 369 Fulham Road, London SW10 9NH, United Kingdom.
Email: i.nagy@imperial.ac.uk

Funding information
Wellcome Trust, Grant number: 061637/Z/06/Z; National Institutes of Health, Grant numbers: DA011322 and DA021696; Fundação para a Ciência e a Tecnologia, Portugal; European Union Marie Curie Intra-European Fellowship, Grant number: 254661; Hungarian Social Renewal Operation Program, Grant number: TÁMOP 4.1.2. E-13/1/KONV-2013-0010; Chelsea and Westminster Health Charity; British Journal of Anaesthesia/Royal College of Anaesthetists Project Grant; Hungarian Academy of Sciences Janos Bolyai Research Fellowship; Hungarian Scientific Research Fund (OTKA), Grant number: K-101873

Abstract

Elevation of intracellular Ca^{2+} concentration induces the synthesis of N-arachydonoylethanolamine (anandamide) in a subpopulation of primary sensory neurons. N-acylphosphatidylethanolamine phospholipase D (NAPE-PLD) is the only known enzyme that synthesizes anandamide in a Ca^{2+}-dependent manner. NAPE-PLD mRNA as well as anandamide's main targets, the excitatory transient receptor potential vanilloid type 1 ion channel (TRPV1), the inhibitory cannabinoid type 1 (CB1) receptor, and the main anandamide-hydrolyzing enzyme fatty acid amide hydrolase (FAAH), are all expressed by subpopulations of nociceptive primary sensory neurons. Thus, NAPE-PLD, TRPV1, the CB1 receptor, and FAAH could form an autocrine signaling system that could shape the activity of a major subpopulation of nociceptive primary sensory neurons, contributing to the development of pain. Although the expression patterns of TRPV1, the CB1 receptor, and FAAH have been comprehensively elucidated, little is known about NAPE-PLD expression in primary sensory neurons under physiological and pathological conditions. This study shows that NAPE-PLD is expressed by about one-third of primary sensory neurons, the overwhelming majority of which also express nociceptive markers as well as the CB1 receptor, TRPV1, and FAAH. Inflammation of peripheral tissues and injury to peripheral nerves induce differing but concerted changes in the expression pattern of NAPE-PLD, the CB1 receptor, TRPV1, and FAAH. Together these data indicate the existence of the anatomical basis for an autocrine signaling system in a major proportion of nociceptive primary sensory neurons and that alterations in that autocrine signaling by peripheral pathologies could contribute to the development of both inflammatory and neuropathic pain.

KEYWORDS
cannabinoid type 1 receptor, fatty acid amide hydrolase, inflammation, neuropathy, pain, transient receptor potential vanilloid type 1 ion channel

1 | INTRODUCTION

N-arachidonoylethanolamine (anandamide) is a lipid signaling molecule (Devane et al., 1992) that is synthesized both in a Ca^{2+}-insensitive and in a Ca^{2+}-sensitive manner through multiple enzymatic pathways and a single pathway that involves the activity of N-acylphosphatidylethanolamine phospholipase D (NAPE-PLD; Okamoto, Morishita, Tsuboi, Tonai, & Ueda, 2004; Ueda, Liu, & Yamanaka, 2001; Wang et al., 2006; Wang, Okamoto, Tsuboi, & Ueda, 2008). Although anandamide acts on a series of molecules, the transient receptor potential vanilloid type 1 ion channel (TRPV1; Caterina et al., 1997) and the cannabinoid 1 (CB1) receptor (Matsuda, Lolait, Brownstein, Young, & Bonner, 1990) are believed to be anandamide's main targets (Devane et al., 1992; Zygmunt et al., 1999). Activation of TRPV1 results in the opening of this nonselective cationic channel and subsequent excitation of nociceptive primary sensory neurons, whereas activation of the CB1 receptor is believed to produce an inhibitory effect that includes the inhibition of L-, P/Q-, and N-type voltage-gated Ca^{2+} channels in neurons, including primary sensory neurons (Caterina et al., 1997; Mackie & Hille, 1992; Mackie, Lai, Westenbroek, & Mitchell, 1995; Tominaga et al., 1998; Twitchell, Brown, & Mackie, 1997). The CB1 receptor and TRPV1 are coexpressed by various neurons, including a great proportion of nociceptive primary sensory neurons (Agarwal et al., 2007; Ahluwalia, Urban, Capogna, Bevan, & Nagy, 2000; Binzen et al., 2006; Mitrirattanakul et al., 2006). This anatomical arrangement allows exogenous anandamide to control the activity of neurons, including a major group of nociceptive primary sensory neurons (Ahluwalia, Urban, Bevan, & Nagy, 2003).

Anandamide is synthesized in subpopulations of primary sensory neurons in both Ca^{2+}-sensitive and Ca^{2+}-insensitive manners (van der Stelt et al., 2005; Varga et al., 2014; Vellani et al., 2008). Consistent with the ability of a group of primary sensory neurons to synthesize anandamide in a Ca^{2+}-sensitive manner (van der Stelt et al., 2005) and the role of NAPE-PLD in such anandamide synthesis (Okamoto et al., 2004; Ueda et al., 2001; Wang et al., 2006, 2008), NAPE-PLD mRNA is expressed by primary sensory neurons (Nagy et al., 2009). Most of the NAPE-PLD mRNA-expressing cells are capsaicin sensitive (Nagy et al., 2009), so they should also express TRPV1 and the CB1 receptor (Agarwal et al., 2007; Ahluwalia et al., 2000; Binzen et al., 2006; Mitrirattanakul et al., 2006). Therefore, in addition to exogenous anandamide, anandamide of primary sensory neuron origin could also be able to control TRPV1 and CB1 receptor activity in a major subpopulation of nociceptive primary sensory neurons in an autocrine manner (van der Stelt & Di Marzo, 2005; van der Stelt et al., 2005).

In addition to NAPE-PLD and the CB1 receptor, the great majority of TRPV1-expressing primary sensory neurons also express the main anandamide-hydrolyzing enzyme fatty acid amide hydrolase (FAAH; Cravatt et al., 1996; Lever et al., 2009). Blocking FAAH activity through increasing the level of anandamide also results in regulating the activity of a proportion of nociceptive primary sensory neurons through the CB1 receptor and TRPV1 (Lever et al., 2009). Based on the coexpression pattern of TRPV1, the CB1 receptor, NAPE-PLD, FAAH, and the effects of those molecules, the presence of an endocannabinoid/endovanilloid autocrine signaling system built by those molecules has been proposed in a major subpopulation of nociceptive primary sensory neurons (Sousa-Valente, Varga, Ananthan, Khajuria, & Nagy, 2014; van der Stelt & Di Marzo, 2005; van der Stelt et al., 2005). That autocrine signaling system, through TRPV1- and CB1 receptor-mediated changes in the intracellular Ca^{2+} concentration and subsequent NAPE-PLD-mediated anandamide synthesis as well as FAAH-mediated anandamide hydrolysis, is considered to be prominently suitable to provide a significant control over TRPV1 and CB1 receptor activity in and, hence, over the excitation of a major group of nociceptive primary sensory neurons (Sousa-Valente, Varga, Ananthan, K., Khajuria, A., & Nagy, I. 2014; van der Stelt & Di Marzo, 2005; Varga et al., 2014).

The excitation level of nociceptive primary sensory neurons is pivotal for the initiation and maintenance of pain experiences, including those that are associated with peripheral pathologies, such as inflammation of peripheral tissues and injury to peripheral nerves (Nagy, Santha, Jancso, & Urban, 2004; Sousa-Valente, Andreou, Urban, & Nagy, 2014). Therefore, the control provided by the endocannabinoid/endovanilloid autocrine signaling system built by the CB1 receptor, TRPV1, NAPE-PLD, and FAAH in a major group of nociceptive primary sensory neurons might play an important role in the development and maintenance of pain. Although the expression patterns and the changes in those expression patterns by pathological conditions of the CB1 receptor, TRPV1, and FAAH have been comprehensively elucidated (Amaya et al., 2004, 2006; Bar, Schaible, Brauer, Halbhuber, & von Banchet, 2004; Hudson et al., 2001; Ji, Samad, Jin, Schmoll, & Woolf, 2002; Lever et al., 2009; Luo, Cheng, Han, & Wan, 2004; Malek et al., 2015; Mitrirattanakul et al., 2006; Yu et al., 2008; Zhou, Li, & Zhao, 2003), little is known about those properties and changes of NAPE-PLD. Therefore, to improve our understanding of the putative autocrine cannabinoid/endovanilloid signaling in primary sensory neurons, this article describes the coexpression patterns of NAPE-PLD with TRPV1, the CB1 receptor, and FAAH under naive conditions and changes in those expression patters under pathological conditions. Preliminary findings were reported earlier by Valente et al. (2011).

2 | METHODS AND MATERIALS

Forty-two male Wistar rats (250–300 g) and 10 C57BL/6 wild-type (WT) and 10 NAPE-PLD$^{-/-}$ (Leung, Saghatelian, Simon, & Cravatt, 2006; Tsuboi et al., 2011) adult mice were used in this study. NAPE-PLD$^{-/-}$ mice were generated by the deletion of a sequence (from

amino acids 99–313) that contains the catalytic domain of the enzyme (Leung et al., 2006; Tsuboi et al., 2011). Both WT and NAPE-PLD$^{-/-}$ mice have been used for antibody control purposes. All quantitative assessments on NAPE-PLD expression pattern have been performed on rat tissues.

All procedures were performed according to the United Kingdom Animals (Scientific Procedures) Act 1986, the revised National Institutes of Health *Guide for the care and use of laboratory animals*, the Directive 2010/63/EU of the European Parliament and of the Council on the Protection of Animals Used for Scientific Purposes, and the guidelines of the committee for research and ethical issues of IASP (Zimmerman, 1983). Furthermore, we fully followed good laboratory practice and ARRIVE guidelines, and every effort was taken to minimize the number of animals used.

2.1 | Rat models of inflammatory and neuropathic pain

Tissue inflammation was induced by injecting 50 μl of 50% complete Freund's adjuvant (CFA; Thermo Scientific, Billerica, MA) or incomplete Freund's adjuvant (IFA; Thermo Scientific) subcutaneously into the plantar aspect of the left hind paw of adult rats. The injection was performed under isoflurane-induced anesthesia.

Nerve injury was produced according to previously published protocols (Kim & Chung, 1992). Briefly, rats were deeply anesthetized with isoflurane, and the fifth lumbar (L5) spinal nerve was exposed and identified after partial laminectomy. A tight 4.0 ligature was then placed around the nerve. The nerve was cut about 5 mm distal from the ligature, and the wound was closed in layers. The sham operation consisted of exposing the L5 spinal nerve without placing the ligature or cutting the nerve.

2.2 | Testing pain-related behavior

Inflammation- or nerve injury-induced changes in responses to mechanical stimuli were assessed with an electrical von Frey apparatus (Ugo Basile, Gemonio, Italy). Briefly, rats were placed in a Perspex chamber with a 0.8-cm-diameter mesh flooring and allowed to acclimatize for 15 min. The tip of the probe was pressed against the plantar surface of the paw at a steadily increasing pressure until the animal voluntarily withdrew the paw. The paw-withdrawal threshold was defined as the average weight in grams over three applications. Care was given not to repeat testing on the same paw within 5 min. Responses to mechanical stimuli were assessed every day for 2 days prior to and 3 days after the injection of either CFA or IFA. In animals that were subjected to nerve injury, changes in the sensitivity to mechanical stimulation were assessed every day for 2 days prior to the surgery and then on the second, fourth, and seventh days after the surgery.

Inflammation- or nerve injury-induced changes in responses to noxious heat stimuli were assessed by the Hargreaves test (Hargreaves, Dubner, Brown, Flores, & Joris, 1988). Briefly, rats were placed in a Perspex box. After a 15-min acclimatization period, an infrared beam (Ugo Basile), which is able to deliver a constantly increasing thermal stimulus, was directed to the plantar surface of the paw. The time until the animal voluntarily withdrew the paw was measured. Again, attention was given not to repeat testing on the same paw within 10 min. Responses to heat and mechanical stimuli were assessed on the same days.

2.3 | Reverse transcription polymerase chain reaction

Rats were killed with isoflurane, and L4 and L5 dorsal root ganglia (DRG) were collected in RNAlater (Sigma-Aldrich, St. Louis, MO) and homogenized with QIA shredder columns (Qiagen, Manchester, United Kingdom). Total RNA was extracted with an RNeasy Plus Mini kit (Qiagen) according to the manufacturer's instruction. RNA was reverse-transcribed with SuperScript II cDNA synthesis reagents (Invitrogen, Carlsbad, CA). Sequences of the primers (Eurofins MWG Operon, Regensburg, Germany) designed to amplify rat NAPE-PLD (NM_199381.1) are forward: TACCAACATGCTGACCCAGA; reverse: ATCGTGACTCTCCGTGCTTC. Sequences of primers designed to amplify the housekeeping gene glyceraldehyde-3-phosphate dehydrogenase (GAPDH; NC_005103) are forward: ACCCATCACCATCTTCCA; reverse, CATCACGCCACAGCTTTCC. The annealing temperature was 57°C; product sizes were 199 bp for NAPE-PLD and 380 bp for GAPDH. The polymerase chain reaction (PCR) mixture was composed of cDNA, primers, 1.5 mM $MgCl_2$, 1 × Green Go-Taq reaction buffer (Promega, Madison, WI), 0.2 mM deoxynucleotide mix (Promega), and 1.25 U Go-Taq DNA polymerase (Promega); the number of cycles was 30. After amplification, PCR products were separated by electrophoresis on 2% agarose gels and visualized with ethidium bromide in Syngene G:Box (Synoptics, Cambridge, United Kingdom). Images were analyzed in Syngene's GeneTools software (Synoptics).

2.4 | Western blotting

Rats and mice were killed with isoflurane, and L4 and L5 DRG were collected and homogenized on ice in NP40 cell lysis buffer (Invitrogen) supplemented with a protease inhibitor cocktail (Sigma-Aldrich). The protein content of the samples was determined with the BCA protein assay reagent (Pierce Biotechnology, Rockford, IL). Proteins were denatured at 95°C for 10 min with 4 × concentrated NuPAGE LDS sample buffer (Invitrogen), after which they were run in a NuPAGE Novex 4–12% Bis-Tris gel (Invitrogen) and blotted onto a PVDF membrane with the iBlot dry blotting system (Invitrogen). To visualize NAPE-PLD, the membrane was first incubated in 5% nonfat milk and then in an anti-NAPE-PLD antibody (1:1,000; Aviva Systems Biology, San Diego, CA) overnight at 4°C. The anti-NAPE-PLD antibody has been raised against the 71–130-amino-acid sequence of the protein (TWKNPSIPNVLRWLI MEKDHSSVPSS KEELDKELPVLKPYFITNPEEAGV). Forty-four percent of this sequence is missing in NAPE-PLD$^{-/-}$ mice (Leung et al., 2006; Tsuboi et al., 2011).

After the membranes had been incubated in the anti-NAPE-PLD antibody, they were incubated with horseradish peroxidase-conjugated goat anti-rabbit secondary antibody (1:1,000; Cell Signaling Technology, Danvers, MA) for 1 hr at room temperature. Western blotting luminol

reagent (Santa Cruz Biotechnology, Santa Cruz, CA) was used for visualization. Images were captured in Syngene G:Box and analyzed in Syngene's GeneTools software. Membranes were then stripped with 0.2 M glycine stripping buffer supplemented with 0.5% Tween-20 (pH 3.0) at room temperature for 30 min and reprobed with rabbit anti-β-actin as a loading control (1:1,000; Cell Signaling Technology).

2.5 | Immunostaining

Animals were killed by intraperitoneal injection of sodium pentobarbital (60 mg/kg) and perfused through the ascending aorta with 100 ml of 0.9% saline, followed by 300 ml of 4% paraformaldehyde in 0.1 M phosphate buffer (PB; pH 7.4). The cerebellum and L4 and L5 DRG were identified and collected bilaterally. Tissues were postfixed for 4–24 hr at 4°C in 4% paraformaldehyde in 0.1 M PB, cryoprotected in 30% sucrose in 0.1 M PB for 1–2 days at 4°C, embedded in a mounting medium, and cut with a cryostat into sections of 10 μm for DRG tissue or 30 μm for cerebella that were mounted on Superfrost slides.

Slides were washed with PBS containing 0.3% Triton X-100 (PBST) and then incubated with PBST containing 10% normal donkey serum (Jackson Immunoresearch, West Grove, PA) for 1 hr at room temperature. Slides were then incubated for 24 hr at room temperature in PBST containing 2% NDS and the appropriate primary antibody/antibodies. In addition to the anti-NAPE-PLD antibody described above, the antibodies included anti-NF200 (200-kD neurofilament) antibody (Sigma-Aldrich) clone NE14, anti-calcitonin gene-related peptide (CGRP) antibody (AB22560; Abcam, Cambridge, MA), anti-TRPV1 antibody (A. Avelino laboratory) EDAEVFKDSMVPGEK, anti-CB1 receptor antibody (K. Mackie laboratory) SCNTATCVTHRLAGLLSRSGGVVKDNFVPTNVGSEAF, and anti-FAAH antibody (B. Cravatt laboratory) GAATRARQKQRASLETMDKAVQRFRLQNPDLDS EALLTLPLLQLVQKLQSGELSPEAVFFTYLG KAWEVNKGTNCVTSYLTD CETQLSQAPRQGLLYGVPVSLKECFSYKGHDSTLGLSLNEGMPSESDC VVVQVLKLQGAVPFVHTNVPQSMLSFDCSNPLFGQTMNPWKSSKSP GGSSGGEGALIGSGGSPLGLGTDIGGSIRFPSAFCGICGLKPTGNRLSKS GLKGCVYGQTAVQLSLGP MARDVESLALCLKALLCEHLFTLDPTVPPL PFREEVYRSSRPLRVGYYETDNYTMPSPAMRRALIE TKQRLEAAGHTLIPFLPNNIPYALEVLSAGGLF SDGGRSFLQNFKGDFVDPCLGDLILILR LPSWF KRLLSLLLKPLFPRLAAFLNSMRPRSAEKLWKL QHEIEMYRQS VIAQWKAMNLDVLLTPMLGPALD LNTPGRATGAISYTVLYNCLDFPA GVVPVTTVTAEDDAQMELYKGYFGDIWDIILKKAMKNSVGL PVAVQ CVALPWQEELCLRF MREVEQLMTPQKQPS. In most of the experiments, NAPE-PLD immunostaining was amplified by the tyramide signal amplification (TSA) system (Perkin Elmer Life Sciences, Waltham, MA) instructions. Immunostaining was visualized by 488-nm or 568-nm Alexa Fluor-conjugated streptavidin (1:1,000; Invitrogen) or a fluorophore-conjugated secondary antibody for 1 hr. Previously, we had extensively tested the specificity and selectivity of the anti-TRPV1, anti-CB1, and anti-FAAH antibodies (Cruz et al., 2008; Lever et al., 2009; Veress et al., 2013).

For the TSA amplification, after incubation of sections in the primary antibody, a biotinylated secondary antibody (1:500 biotin donkey anti-rabbit; Jackson Immunoresearch) was applied. Slides were then incubated with peroxidase containing avidin–biotin complex (1:200; ABC kit; Perkin Elmer Life Sciences) for 1 hr. The biotinylated tyramide was detected with fluorescent streptavidin (see above). To control for the combined use of two antibodies raised in the same species in combination with the TSA amplification, the following experiments were conducted: (a) the primary antibody was omitted; (b) a fluorescent secondary antibody recognizing the species in which the primary antibody had been produced was added at the end of the TSA reaction to determine whether any unoccupied primary antibody could generate signal; and (c) for the same primary antibody, a TSA reaction and primary fluorescent secondary antibody reaction were performed in tandem in adjacent sections to verify whether both types of reactions would yield similar results.

In addition to the antibodies, fluorescein-labeled *Griffonia simplicifolia* isolectin B4 (IB4; Sigma-Aldrich) was used to identify the nonpeptidergic subpopulation of nociceptive primary sensory neurons (Silverman & Kruger, 1990). This was performed by incubating sections in a 1:1,000 dilution of the fluorochrome-conjugated IB4 for 1 hr during the final incubation step for NAPE-PLD staining. Slides were mounted in Vectashield medium (Vector Laboratories, Burlingame, CA).

2.6 | Control experiments

For testing the specificity and selectivity of the anti-NAPE-PLD antibody, we first studied proteins identified by the anti-NAPE-PLD antibody in protein samples prepared from the cerebella of WT and NAPE-PLD$^{-/-}$ mice. Furthermore, we studied the immunostaining generated by the anti-NAPE-PLD antibody in sections that had been cut from DRG and cerebellum of WT and NAPE-PLD$^{-/-}$ mice. Finally, we studied the proportion and size distribution of cells expressing NAPE-PLD mRNA as well as the coexpression pattern between NAPE-PLD mRNA and NAPE-PLD protein (vide infra).

2.7 | Fluorescent in situ hybridization

Fluorescent in situ hybridization was carried out with a custom Stellaris FISH probe kit, which contains 48 fluorescent dye-conjugated NAPE-PLD mRNA complementary short probes (Biosearch Technologies, Petaluma, CA). All material and stock solutions were treated with diethyl pyrocarbonate (DEPC; Sigma-Aldrich) or RNase ZAP (Sigma-Aldrich) or kept at −80°C for 8 hr to prevent RNA degradation. The DEPC treatment included adding 2.5 mM DEPC to all solutions and autoclaving. DRG sections mounted on coverslips were washed with PBS and then permeabilized with 70% ethanol for 1 hr at room temperature. After having been rinsed in washing buffer that contained 20% formamide and 2 × concentrated saline sodium citrate (SSC) buffer that contained sodium chloride and trisodium citrate, slides were incubated with the NAPE-PLD probe (2.5 μM) in hybridization buffer (2 × SSC buffer, 10% formamide, and 100 mg/ml dextran sulfate) at room temperature for 24 hr. On the next day, after a 1-hr incubation in the washing buffer, slides were immunoreacted with the NAPE-PLD antibody as described above. For control, sections were incubated as described above, but the NAPE-PLD probes were omitted from the hybridization buffer.

Control sections were run in parallel with sections incubated in the presence of the NAPE-PLD probes.

2.8 | Image analysis and quantification of immunofluorescent DRG cells

Immunofluorescent images were examined with a Leica (Wetzlar, Germany) DMR Fluorescence, Zeiss (Jena, Germany) Axioscope 40, or Zeiss LSM 700 confocal laser scanning microscope. With the Leica microscope, images were taken by a Hamamatsu CCD camera connected to a PC running QWIN software (Leica). The PC connected to the Zeiss Axioscope 40 ran AxioVision 4.6, whereas the PC connected to the Zeiss LSM 700 microscope ran ZEN software.

With each microscope, corresponding identical acquisition parameters were used and raw, unprocessed images were used for analysis in Image J. Images selected for figures, however, were subjected to contrast and brightness adjustments when we determined that was required.

Neurons that displayed a visible nucleus were identified, and the cytoplasm and the nuclei of these cells were marked as regions of interest (ROI). The area and mean pixel intensity of the ROIs were then measured. At least 200 cells were sampled in each side of each animal in serial sections at a distance of ±10 sections (i.e., 100 μm) apart from one another to ensure that each cell with a given staining was included in the analysis only once.

The threshold staining intensity was established by using three independent methods. First, with visual inspections, we confirmed that sections contained both immunopositive and immunonegative cells. The presence of the two types of neurons was also confirmed by the non normal distribution of the staining intensities in each section (Shapiro-Wilk test). k-Clustering is able to separate variables into a defined number of clusters that then exhibit the greatest possible distinction. Therefore, we used k-clustering to define two clusters and the intensity values that separate the two groups of neurons in each section.

In the second method, raw intensity values were transformed by using a logarithmic equation (LOG[255/(255—value)]). These values were ranked and displayed on a scatterplot. The initial and last linear parts of the plots were then fitted with a tangent, and the intensity value at the intersection of the two fitted lines was used as a threshold to separate labeled and nonlabeled cells. This initial separation was then used in a discriminant analysis as prediction. This statistical probe also confirmed that the accuracy of the prediction was between 95% and 100%.

Finally, one blinded experimenter examined images of randomly chosen sections from naive animals, and the immunopositivity or immunonegativity judged by that experimenter was noted; these notes were then associated with the staining intensity values measured in ImageJ. These combined data were then used to determine the threshold of immunopositivity by the receiver operating curve. The ratio of immunopositive and immunonegative cells determined by the three methods did not differ more than 5%. Data presented throughout the article were obtained with the second method.

In addition to establishing the immunopositive and immunonegative cells, intensity values were also used for studying pathology-induced changes in staining intensities of NAPE-PLD, TRPV1, CB1 receptor, and FAAH immunopositivity as well as pathology-induced changes in the correlation between staining intensities of NAPE-PLD and TRPV1, CB1 receptor, or FAAH immunopositivity.

2.9 | Statistical analysis

For naive animals, data from both the left and the right sides were analyzed and used for further statistical analysis. For treated animals, data obtained from the ipsilateral and the contralateral sides of the same treatment group were averaged, tested for normal distribution (Shapiro–Wilk test), and analyzed for statistical differences. Statistical analysis of behavioral data was performed between withdrawal responses (on different testing days or among different animal groups on the same testing day) by ANOVA, followed by Tukey's test or by two-tailed Student's *t* test, as appropriate. Statistical comparisons among the number of immunostained cells identified in different experimental groups were performed by two-tailed Fisher's exact test. Differences among sizes of neurons belonging to various populations were compared by two-tailed Mann-Whitney U test. All data are expressed as mean ± SEM; "*n*" refers to the number of repeated measurements in each of the experimental groups. $p < .05$ was considered to be statistically significant.

3 | RESULTS

3.1 | NAPE-PLD is expressed in primary sensory neurons of DRG

Gel images of RT-PCR products exhibited detectable levels of NAPE-PLD mRNA in L4–5 rat DRG (Figure 1a). The size of the PCR product was indistinguishable from the expected product size of 199 bp (Figure 1a). These findings support previous data showing that a subpopulation of primary sensory neurons expresses NAPE-PLD (Bishay et al., 2010; Nagy et al., 2009).

To confirm that NAPE-PLD mRNA is expressed in neurons in DRG, we performed fluorescent in situ hybridization in sections cut from rat L4–5 DRG. Analysis of the staining confirmed that NAPE-PLD mRNA is expressed in DRG and that only a subpopulation of neurons expresses this transcript (Figure 1b,c).

To determine whether NAPE-PLD protein is also expressed in rat DRG, we performed Western blotting. The anti-NAPE-PLD antibody (Aviva Systems Biology) we used throughout this study recognized, in addition to some unknown proteins, a protein with the predicted size of NAPE-PLD (~46 kDa) in samples prepared from rat DRG (Figure 2a). In addition, the anti-NAPE-PLD antibody also recognized a protein with the predicted size (~46 kDa) in WT mouse brain (together with, apparently, the same unknown proteins; Figure 2a). However, although the antibody recognized the unknown proteins, it did not recognize the specific ~46-kDa protein in samples prepared from the brains of NAPE-PLD$^{-/-}$ mice (Figure 2a).

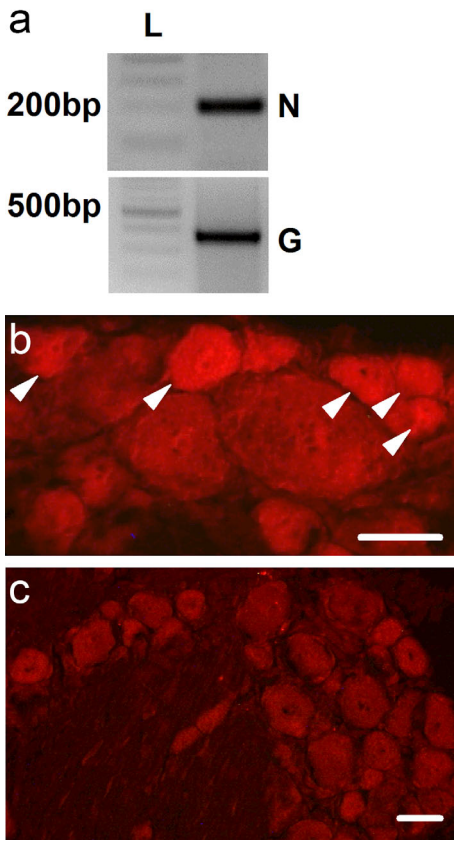

FIGURE 1 The NAPE-PLD transcript is expressed in adult rat DRG. (a) Gel image of RT-PCR products that were synthesized from total RNA isolated from the L4–5 DRG of adult rats with primers designed to amplify NAPE-PLD (N, top) and GAPDH (G, bottom) mRNA. The size of the RT-PCR products is indistinguishable from the predicted size of NAPE-PLD (N, 199 bp) and GAPDH (G, 380 bp). (b) Microphotograph taken from a DRG section of an adult rat following fluorescent in situ hybridization with 48 short NAPE-PLD complementary fluorescent dye-tagged probes. The labeling identified only neurons (arrowheads). The great majority of the positive neurons were small-diameter cells. (c) Microphotograph taken from another rat DRG section that was incubated in parallel with the one shown in B in identical solutions with the exception that the specific in situ probes were omitted from the hybridization buffer. Scale bars = 20 μm in both (b) and (c)

To confirm that the NAPE-PLD protein is expressed exclusively by neurons in DRG, we incubated sections cut from rat L4–5 DRG with the anti-NAPE-PLD antibody and visualized the staining via TSA. Analysis of the immunostaining revealed that the antibody produced a homogenous staining in the cytoplasm of DRG neurons (Figure 2b). In addition to DRG neurons, a fluorescent signal was also seen in some satellite cells (Figure 2b). However, our control experiments revealed that this staining is produced by the TSA reaction when the postfixation time is less than 24 hr (data not shown).

To obtain evidence that the anti-NAPE-PLD antibody produces a selective and specific immunostaining, we immunoreacted cerebellum and DRG sections of WT and NAPE-PLD$^{-/-}$ mice (Figure 3a–d). As expected (Nagy et al., 2009; Suarez et al., 2008), WT mouse Purkinje cells (Figure 3a$_{1-4}$) as well as a subpopulation of WT mouse DRG neurons (Figure 3c$_{1-4}$) exhibited strong NAPE-PLD immunoreactivity. In contrast, the immunoreaction produced by this antibody was lost in both cerebella and DRG dissected from NAPE-PLD$^{-/-}$ mice (Figure 3b$_{1-4}$,d$_{1-4}$).

To provide additional evidence that the anti-NAPE-PLD antibody produces a specific and selective staining, we also combined the immunostaining with in situ hybridization using fluorescent NAPE-PLD probes (Figure 4). Analysis of this combined staining revealed that 73 of 231 cells (31.6%) showed positivity for the in situ probes. The number of cells showing NAPE-PLD immunopositivity was not significantly different from this value (75 of 231 [32.5%], $p = .9$, Fischer's exact test). The proportion of immunopositive neurons was not significantly different from that found in naive animals in the remainder of the study (37.6% ± 0.17%, $n = 18$, $p = .13$, Fischer's exact test). The combined fluorescent in situ hybridization and immunofluorescent staining also revealed that 59 of the total number of neurons showed double staining (25.6%), which represented 80.8% and 78.7% of the in situ- and immunopositive cells, respectively.

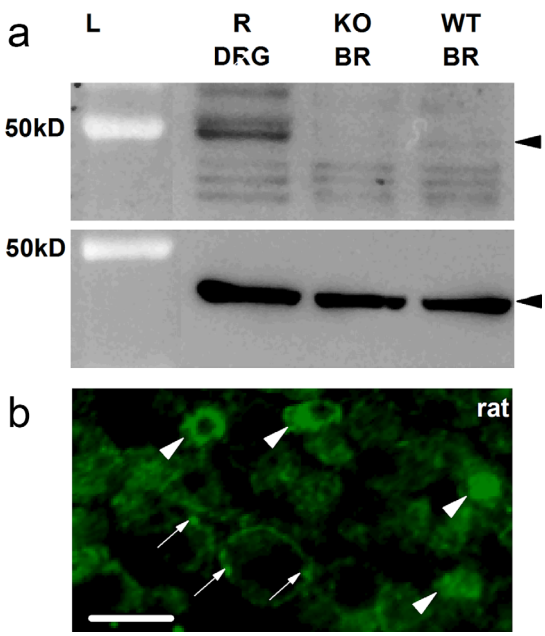

FIGURE 2 The NAPE-PLD protein is expressed in adult rat DRG. (a) A gel image (top) of immunoblots with an antibody raised against NAPE-PLD and protein samples prepared from rat DRG (R/DRG), NAPE-PLD$^{-/-}$ mouse brain (KO/BR), or WT mouse brain (WT/BR). In addition to recognizing a protein with the predicted size of NAPE-PLD (~46 kD) in rat DRG and WT mouse brain tissues, the antibody also recognized some unknown proteins in all samples. However, the antibody failed to recognize the protein with the predicted size of NAPE-PLD in NAPE-PLD$^{-/-}$ mouse brain. Bottom image shows β-actin (42 kD) expression as loading control. (b) Microphotograph of a section cut from a rat DRG. The anti-NAPE-PLD antibody produced staining in a subpopulation of primary sensory neurons (arrowheads). In addition, satellite cells visible occasionally around primary sensory neurons also exhibit NAPE-PLD immunopositivity (arrows). However, control experiments revealed that this staining is produced by the TSA reaction when the postfixation time is less than 24 hr. Scale bar = 30 μm

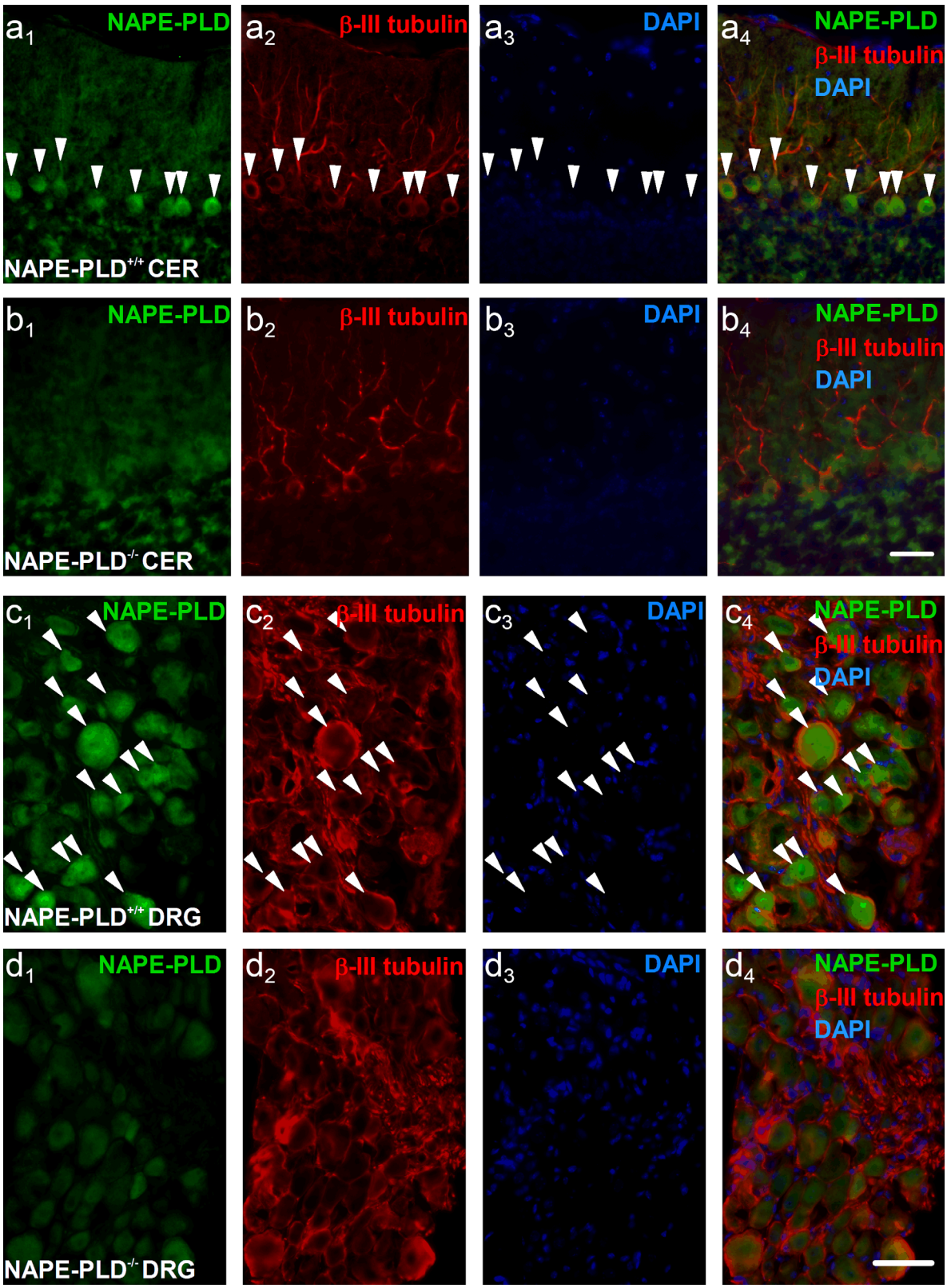

FIGURE 3.

3.2 | NAPE-PLD is expressed in small DRG neurons

Next, we analyzed the morphology and neurochemical properties of NAPE-PLD-expressing primary sensory neurons. Among the 8,129 DRG neurons that we analyzed, 3,056 were NAPE-PLD immunoreactive (37.60% ± 0.17%, ipsilateral and contralateral sides of nine animals, $n = 18$ repeated measurements; Table 1). The cell size distribution of

NAPE-PLD-immunostained neurons revealed that most of the NAPE-PLD-expressing cells were small neurons, although some large NAPE-PLD-immunopositive cells were also found (Figure 5). The area of perikarya of the NAPE-PLD-immunoreactive cells was $923 \pm 9\,\mu m^2$ ($n = 3{,}056$). This value was significantly smaller than the average area of perikarya of unlabeled cells ($1{,}315 \pm 10\,\mu m^2$, $n = 5{,}073$, $p = .01$, two-tailed Mann Whitney U test).

3.3 | NAPE-PLD is expressed by both peptidergic and nonpeptidergic nociceptive neurons

The great majority of small-diameter primary sensory neurons are nociceptive in function (Nagy, Santha, Jancso, & Urban, 2004). Although nociceptive primary sensory neurons either contain neuropeptides such as CGRP or express the binding site for the lectin IB4, non nociceptive neurons express the heavy (200 kDa) neurofilament NF200 (Lawson, Harper, Harper, Garson, & Anderton, 1984; Lawson & Waddell, 1991). Therefore, to confirm that NAPE-PLD-expressing DRG neurons are indeed nociceptive, we used combined immunofluorescent staining with the anti-NAPE-PLD antibody (an anti-NF200) and an anti-CGRP antibody as well as fluorescein-conjugated IB4 on sections cut from L4–5 DRG. The results of these combined immunoreactions are shown in Figure 6 and Table 1. In summary, 31.28% ± 3.89% ($n = 6$) of the NAPE-PLD immunoreactive neurons expressed NF200 (154 of 502 cells in the left and right sides of three animals; Figure 6a–c, Table 1). In contrast, 52.05% ± 2.02% ($n = 6$) of the cells bound IB4 (267 of 512 cells in the left and right sides of three animals; Figure 6d–f, Table 1), and 34.58% ± 2.67% ($n = 6$) of the cells exhibited immunopositivity for the neuropeptide CGRP (174 of 509 cells in the left and right sides of three animals; Figure 6g–i, Table 1). It is important to note that more NAPE-PLD-expressing cells bound IB4 than contained CGRP ($p < .001$, Fisher's exact test).

3.4 | NAPE-PLD shows a high level of coexpression with TRPV1, the CB1 receptor, and FAAH

To discover whether NAPE-PLD could indeed be involved in the formation of an autocrine endocannabinoid/endovanilloid signaling system in a subpopulation of primary sensory neurons, we next assessed the coexpression of NAPE-PLD and FAAH, the CB1 receptor, or TRPV1. Data from the analysis of these combined immunoreactions are shown in Figure 7 and Table 1. In summary, we found a very high level of coexpression between NAPE-PLD and all the endocannabinoid/endovanilloid signaling-related molecules (Figure 7, Table 1). However, significantly more ($p = .029$, Fisher's exact test) NAPE-PLD-immunopositive neurons expressed the CB1 receptor (72.71% ± 1.47%, $n = 6$, 349 of 480 cells in three animals) than TRPV1 (59.89% ± 1.33%, $n = 6{,}304$ of 546 cells in the left and right sides of three animals).

We also assessed the correlation between the intensities of NAPE-PLD and the CB1 receptor, TRPV1, or FAAH immunostaining. Although NAPE-PLD and CB1 receptor immunostaining exhibited a high correlation ($R = .76 \pm .02$, $n = 3$; Figure 8a), essentially no correlation was found between NAPE-PLD and TRPV1 immunostaining ($R = .14 \pm .07$, $n = 3$; Figure 8b). Furthermore, a weak correlation ($R = .34 \pm .06$, $n = 3$; data not shown) was found between the intensities of NAPE-PLD and FAAH immunoreactivity.

3.5 | Both CFA and IFA injection induce changes in NAPE-PLD, TRPV1, and the CB1 receptor immunolabeling pattern

In primary sensory neurons, one of the main functions of anandamide's excitatory target, TRPV1, is to signal peripheral inflammatory events to the central nervous system (Nagy, Friston, Valente, Perez, & Andreou, 2014; White, Urban, & Nagy, 2011). To determine whether peripheral inflammation induces changes in NAPE-PLD expression that may be associated with increased TRPV1 activity, after the assessment of behavioral changes, we studied the expression pattern of NAPE-PLD, TRPV1, the CB1 receptor, and FAAH after the induction of inflammation in the hind paw.

CFA injection into the hind paw produced hypersensitivity to both thermal and mechanical stimuli 3 days after injection, which was significantly greater than that induced by IFA (data not shown). The proportion of NAPE-PLD immunostained neurons was significantly reduced by both CFA and IFA injections on the ipsilateral side (from 37.60% ± 0.17% [3,056/8,129 cells in the left and right sides of nine animals], $n = 18$, to 35.18% ± 0.64% [1,363/3,872 in the ipsilateral side of three animals], $p = .01$, Fisher's exact test, by IFA and to 35.40% ± 0.60%

FIGURE 3 The NAPE-PLD antibody provides specific and selective staining. (a_{1-4}) Microphotographs (taken with the Zeiss Axiotome microscope) of a section cut from a WT mouse (NAPE-PLD$^{+/+}$) cerebellum and immunostained with the combination of an anti-NAPE-PLD (a_1, green) and an anti-β-III tubulin (a_2, red) antibody. The section was also stained with DAPI (a_3, blue). (a_4) shows a composite image of (a_{1-3}). Consistent with previous findings, the perikarya of Purkinje cells show strong immunopositivity for NAPE-PLD (arrowheads). (b_{1-4}) Microphotographs (taken with the Zeiss Axiotome microscope) of a section cut from the cerebellum of a NAPE-PLD$^{-/-}$ mouse and immunoreacted with the mixture of the anti-NAPE-PLD (b_1) and the anti-β-III tubulin (b_2) antibodies. The section was also stained by DAPI (b_3). (b_4) shows a composite image of (b_{1-3}). Note the complete lack of immunolabeling by the anti-NAPE-PLD antibody. (c_{1-4}) Microphotographs (taken with the Zeiss Axiotome microscope) of a section cut from a WT mouse DRG and immunostained with the mixture of the anti-NAPE-PLD (c_1) and the anti-β-III tubulin (c_2) antibodies. The section was also stained by DAPI (c_3). (c_4) shows a composite image of (c_{1-3}). The immunoreaction produced staining in a subpopulation of neurons (arrowheads). (d_{1-4}) Microphotographs (taken with the Zeiss Axiotome microscope) of a section cut from a NAPE-PLD$^{-/-}$ mouse DRG and immunostained with the mixture of the anti-NAPE-PLD (d_1) and the anti-β-III tubulin (d_2) antibodies. The section was also stained by DAPI (d_3). (d_4) shows a composite image of (d_{1-3}). Note the complete lack of NAPE-PLD immunopositivity. Images of DRG sections are stack images from eight images of 1.25 μm each. Images of the cerebellum are stack images from 12 images of 1.42 μm each. Scale bars = 50 μm

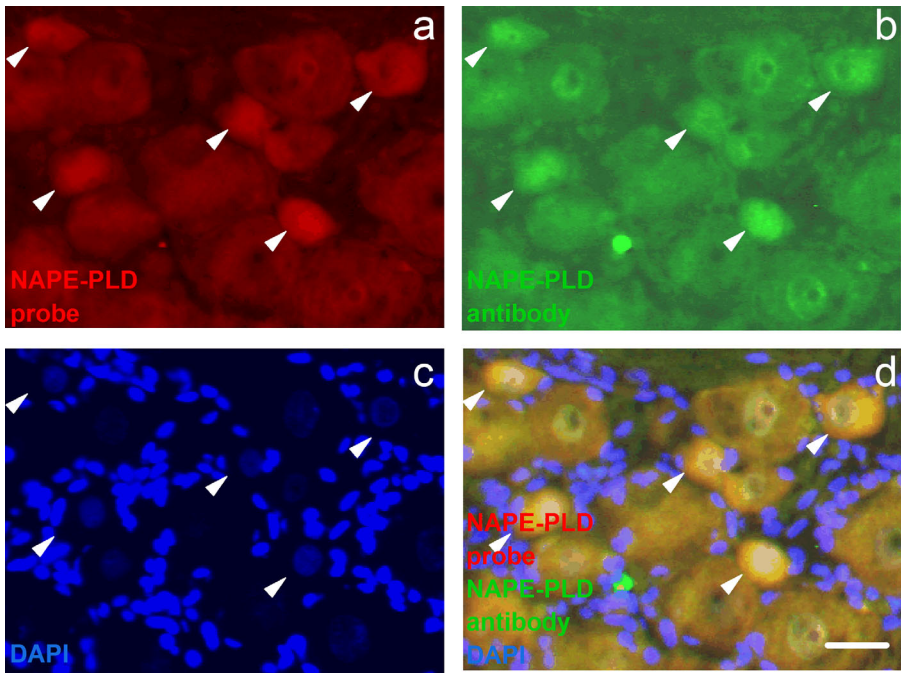

FIGURE 4 Combined staining with NAPE-PLD in situ probes and the anti-NAPE-PLD antibody reveals a high degree of costaining. (a) Microphotograph shows the result of fluorescent in situ hybridization in a rat DRG section with fluorescent dye-tagged probes specific for NAPE-PLD mRNA. Labeling identified a group of neurons (arrowheads). (b) Microphotograph shows the image of the same cells shown in A immunolabeled with the anti-NAPE-PLD antibody. Arrowheads indicate NAPE-PLD-immunopositive cells. (c) Microphotograph of the visual field shown in A and B but stained with DAPI. (d) Composite image of A–C. Arrowheads indicate double-labeled cells. In this visual filed, the costaining of neurons is 100%. Scale bar = 20 μm

[1,483/4,181 cells in the ipsilateral side of three animals], $p = .02$, Fisher's exact test, by CFA; Figure 9, Table 2) but not on the contralateral side. The cell size distribution of the NAPE-PLD-immunopositive cells was not changed on either the ipsilateral side or the contralateral side (data not shown). The high correlation between NAPE-PLD and CB1 receptor immunostaining intensity was significantly reduced by both CFA injection (from 0.76 ± 0.02 [$n = 3$] to 0.48 ± 0.03 [$n = 3$], $p < .001$, Student's t-test; Figure 8c) and by IFA injection (from 0.76 ± 0.02 [$n = 3$] to 0.57 ± 0.02 [$n = 3$], $p < .001$, Student's t-test; data not shown) on the ipsilateral side but not on the contralateral side. Furthermore, the ipsilateral/contralateral ratios of NAPE-PLD, CB1 receptor, and FAAH immunostaining were not changed (Figure 8d). However, the ipsilateral/contralateral ratio for TRPV1 immunolabeling was increased by both IFA injection (from 1 ± 0.03 [$n = 3$] in naive to 1.21 ± 0.07 [$n = 3$] in IFA-injected animals, $p = .02$, Student's t test; data not shown) and CFA injection (from 1 ± 0.03 [$n = 3$] in naive to 1.16 ± 0.05 [$n = 3$] in CFA-injected animals, $p = .03$, Student's t test; Figure 8d).

3.6 | Spinal nerve ligation results in a pronounced reduction of NAPE-PLD immunoreactivity in injured DRG neurons

Nerve injury has been associated with changes in expression in many proteins, including various components of the endocannabinoid/endovanilloid systems and in anandamide levels in DRG (Agarwal et al.,

TABLE 1 Summary of the proportion of neurons expressing NAPE-PLD and other markers in L4–5 DRG of naive animals

	Number of cells used for analysis	Percentage of neurons expressing various markers	Percentage of NAPE-PLD-expressing cells expressing various markers	Percentage of neurons expressing various markers together with NAPE-PLD
NAPE-PLD	8,129	38 ± 0.3	-	-
NF200	1,313	37 ± 0.5	31 ± 3.9	32 ± 3.3
IB4	1,361	34 ± 0.6	52 ± 2.0	57 ± 2.1
CGRP	1,374	38 ± 0.5	35 ± 2.7	34 ± 2.8
TRPV1	1,350	42 ± 0.7	60 ± 1.3	54 ± 2.3
CB1	1,267	34 ± 0.6	73 ± 1.5	82 ± 1.6
FAAH	1,464	34 ± 1.2	62 ± 2.8	67 ± 3.3

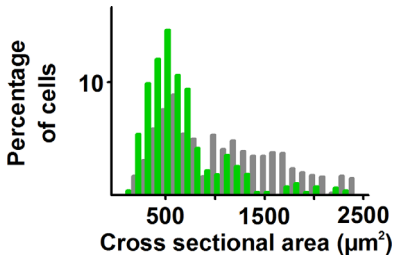

FIGURE 5 Most primary sensory neurons expressing NAPE-PLD are small cells. Cell size distribution of NAPE-PLD-immunopositive (green bars) and -immunonegative (gray bars) rat DRG neurons. The great majority of the NAPE-PLD-immunopositive cells are small cells, although some larger cells also express NAPE-PLD [Color figure can be viewed at wileyonlinelibrary.com]

2007; Costigan et al., 2002; Hudson et al., 2001; Lever et al., 2009; Michael & Priestley, 1999; Zhang, Zhao, Jiang, Wang, & Ma, 2007). Therefore, we next assessed nerve injury-induced alterations in NAPE-PLD, FAAH, TRPV1 and CB1 receptor expression.

In agreement with previous results (Kim & Chung, 1992), ligation and transection of the fifth lumbar spinal nerve but not sham surgery resulted in the development of reflex hypersensitivity to mechanical and thermal stimuli from 2 to 7 days after the surgery (data not shown). Both the nerve injury and the sham surgery resulted in significant reductions in the number of NAPE-PLD-immunostained neurons in the injured DRG (from 37.60% ± 0.17% [3,056 of 8,129 cells in the left and right sides of nine animals, $n = 18$] to 33.71% ± 2.19% [653 of 1,932 cells in three sets of samples, that is, three different combined stainings from the ipsilateral side of three animals, $n = 9$, $p = .002$,

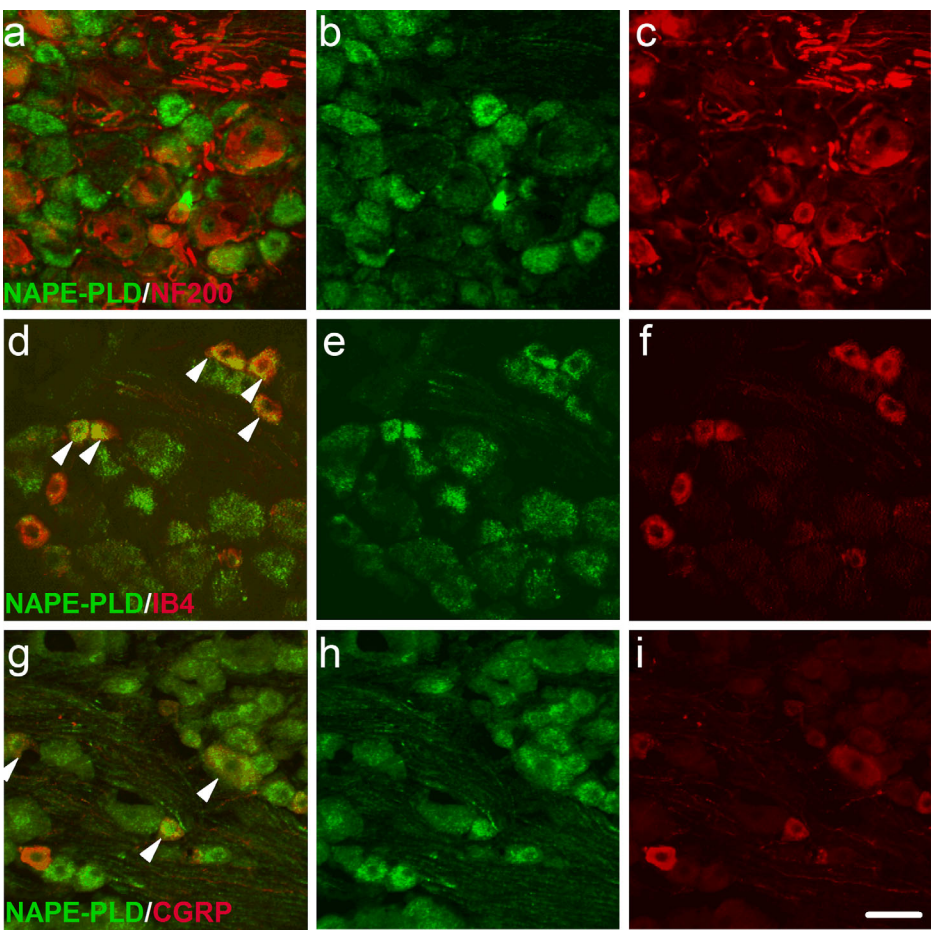

FIGURE 6 Most primary sensory neurons expressing NAPE-PLD also express markers for nociceptive primary sensory neurons. Combined immunolabeling was produced by using the anti-NAPE-PLD antibody with an antibody raised against the 200-kD neurofilament NF200 (a–c), with biotinylated IB4 (d–f), or with an antibody raised against CGRP (g–i). (a–c) show a typical combined image (a) and separated images (b,c) of a section incubated with the anti-NAPE-PLD (b, green) and an anti-NF200 (c, red) antibody. NAPE-PLD shows a low degree of coexpression with NF200. (d–f) show a typical combined image (d) and separated images (e,f) of a section incubated with the anti-NAPE-PLD antibody (e, green) and a biotinylated IB4 (red; f). NAPE-PLD shows a high degree of coexpression with the IB4 binding site. (g–i) show a typical combined image (g) and separated images (h,i) of a section incubated with the anti-NAPE-PLD (h, green) and anti-CGRP antibody (i, red). NAPE-PLD also shows coexpression with CGRP. Arrowheads in (d) and (g) indicate NAPE-PLD/IB4-binding site-expressing neurons and NAPE-PLD/CGRP-immunopositive neurons, respectively. For quantified data, see Table 1. All images are single scan images acquired with a ×20 objective lens (NA: 0.50) and a 47-μm pinhole aperture corresponding to 1.29 Airy units, providing four 6-μm-thin optical sections. Scale bar = 50 μm

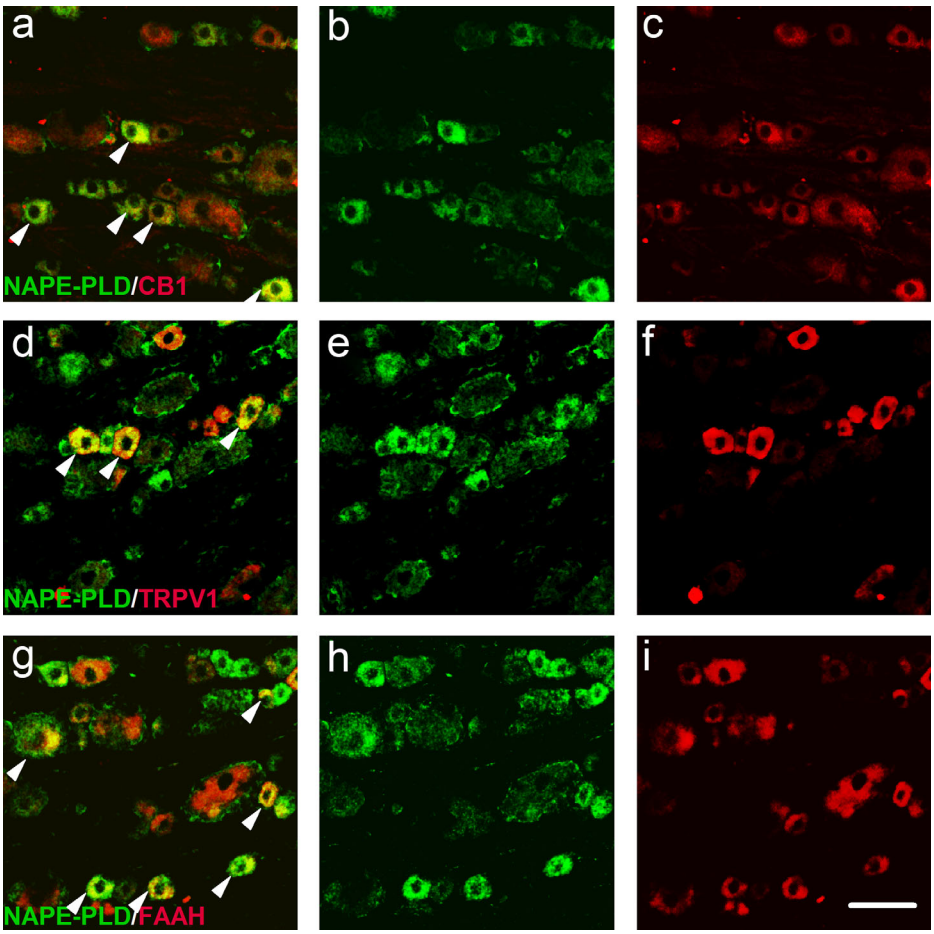

FIGURE 7 Most primary sensory neurons expressing NAPE-PLD also express the CB1 receptor, TRPV1, and/or FAAH. (a–c) Typical combined image (a) and separated images (b,c) of a section incubated with the anti-NAPE-PLD (b, green) and an anti-CB1 receptor (c, red) antibody. NAPE-PLD shows a high degree of coexpression with the CB1 receptor. (d–f) A typical combined image (d) and separated images (e,f) of a section incubated with the anti-NAPE-PLD (e, green) and an anti-TRPV1 (f, red) antibody. NAPE-PLD also shows a high degree of coexpression with TRPV1. (g–i) A typical combined image (g) and separated images (h,i) of a section incubated with the anti-NAPE-PLD (h, green) and an anti-FAAH (i, red) antibody. NAPE-PLD also shows a high degree of coexpression with FAAH. Arrowheads in (a, d, g) indicate NAPE-PLD/CB1 receptor-coexpressing, NAPE-PLD/TRPV1-coexpressing, and NAPE-PLD/FAAH-immunopositive neurons, respectively. For quantified data, see Table 1. All images are single scan images acquired with a ×20 objective lens (NA: 0.50) and a 47-μm pinhole aperture corresponding to 1.29 Airy units, providing four 6-μm-thin optical sections. Scale bar = 50 μm

Fischer's exact test by sham surgery] and to 18.50% ± 1.42% [653 of 1,932 cells in three sets of samples from the ipsilateral side of three animals, $n = 9$, $p < .001$, Fischer's exact test by spinal nerve ligation (SNL)]; Figure 10, Table 3), although the SNL-induced reduction was significantly greater than that produced by the sham injury ($p < .001$, Fischer's exact test). SNL but not the sham injury also reduced the number of TRPV1-immunolabeled neurons (from 42.14% ± 0.69% [569 of 1,350 cells in the ipsilateral and contralateral sides of three animals, $n = 6$] to 6.38% ± 6.15% [41 of 695 cells in the ipsilateral side of three animals, $n = 3$], $p < .001$, Fischer's exact test) and CB1 receptor-immunolabeled neurons (from 33.64% ± 0.59% [426 of 1,267 cells in the ipsilateral and contralateral sides of three animals, $n = 6$] to 24.64% ± 8.46% [96 of 653 cells in the ipsilateral side of three animals, $n = 3$], $p < .001$, Fischer's exact test) and increased the number of FAAH-immunolabeled neurons (from 34.39% ± 1.24% [501 of 1,464 cells in the ipsilateral and contralateral sides of three animals, $n = 6$] to 50.81% ± 6.49% [307 of 614 cells in the ipsilateral side of three animals, $n = 3$], $p < .001$, Fischer's exact test) in the injured DRG (Figure 10, Table 3). Both the sham injury (data not shown) and the SNL significantly reduced the correlation between the intensities of NAPE-PLD and CB1 receptor immunolabeling on both the ipsilateral (Figure 8c) and the contralateral (data not shown) sides. Although the number of TRPV1-immunopositive cells was reduced, the ipsilateral/contralateral ratio of TRPV1 immunolabeling was increased (from 1 ± 0.03 [$n = 3$] to 1.29 [$n = 2$]; Figure 8d) however, because of the absence of TRPV1-immunolabeled neurons in one animal, the significance could not be assessed.

Previous research has demonstrated that primary sensory neurons in the DRG adjacent to the injured DRG also show phenotypic changes (Hammond, Ackerman, Holdsworth, & Elzey, 2004; Hudson et al., 2001). Therefore, we also assessed NAPE-PLD, TRPV1, CB1, receptor, and FAAH immunostaining in the ipsilateral L4 DRG. We found no

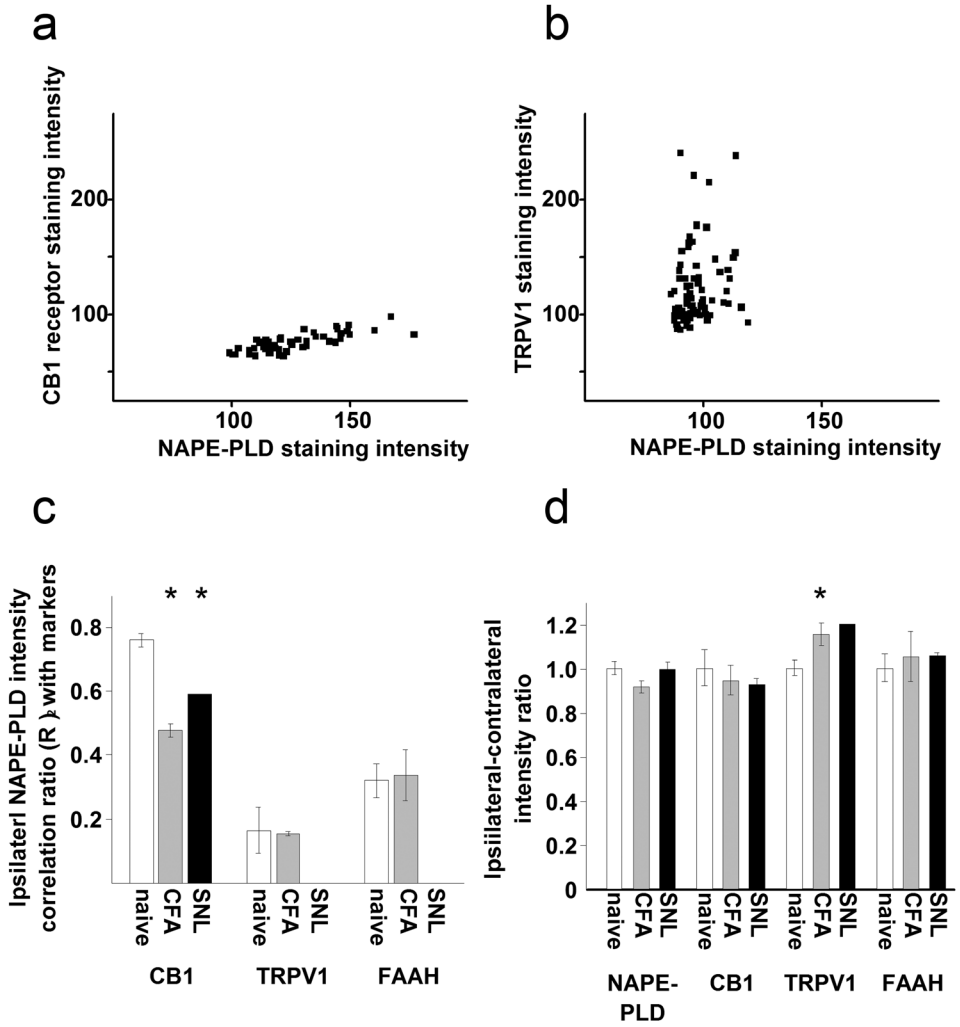

FIGURE 8 Peripheral pathological conditions disturb the staining pattern observed in naive animals. (a) Correlation between NAPE-PLD and CB1 receptor staining intensity of naive rat primary sensory neurons exhibiting coexpression of these two molecules. Note the high correlation between the intensities of the two stainings. (b) Correlation between NAPE-PLD and TRPV1 immunostaining intensity of naive rat primary sensory neurons exhibiting coexpression of these two molecules. Note the lack of correlation between the intensities of the two stainings. (c) Correlation of NAPE-PLD immunostaining with immunostaining intensities for the CB1 receptor, TRPV1, and FAAH in ipsilateral DRG under naive conditions (open bars) following injection of CFA (gray bars) into the paw or following SNL (black bar). Note that the strong correlation between the staining intensities of the NAPE-PLD and CB1 receptor immunostaining observed in naive animals was significantly reduced by both CFA injection and SNL (asterisks). (d) Ratio between staining intensities on the ipsilateral and contralateral DRG for the various markers (NAPE-PLD, the CB1 receptor, TRPV1, and FAAH) under naive conditions (open bars) following CFA injection (gray bars) and following SNL (black bars). Note that CFA injection significantly (asterisk) increases the ipsilateral–contralateral TRPV1 staining intensity. Although SNL appears to have the same effect because of the reduction in the number of TRPV1-immunopositive cells, the ratio could be established only in two animals, and statistical analysis was not performed. All data are expressed as mean ± SEM

significant change in the ratio of immunopositive cells for NAPE-PLD ($p = .415$), FAAH ($p = .454$), or TRPV1 ($p = .166$; two-tailed Fisher's exact test; Table 4). For the CB1 receptor, the significance level for the reduction in the ratio of immunopositive cells was $p = .051$ (Fisher's exact test; Table 4).

4 | DISCUSSION

The present study shows that about one-third of primary sensory neurons in lumbar DRG express NAPE-PLD. The present data also show that about two-thirds to three-quarters of the NAPE-PLD-expressing neurons could be nociceptive because most of the NAPE-PLD-immunopositive cells are small-diameter neurons that are nociceptive in function (Nagy et al., 2004) and that ~35%, ~50%, and ~60% of the NAPE-PLD-expressing cells also express the nociceptive markers CGRP, IB4-binding site, and TRPV1, respectively, (nota bene, CGRP, IB4-binding site, and TRPV1 exhibit significant coexpression in DRG [Nagy et al., 2004]), whereas only ~30% of the cells express the nonnociceptive cell marker heavy weight neurofilament NF200. These data are consistent with recent findings showing that NAPE-PLD mRNA is expressed in primary sensory neurons and that most of those neurons are sensitive to the archetypical TRPV1 activator capsaicin (Bishay et al., 2010; Nagy et al., 2009).

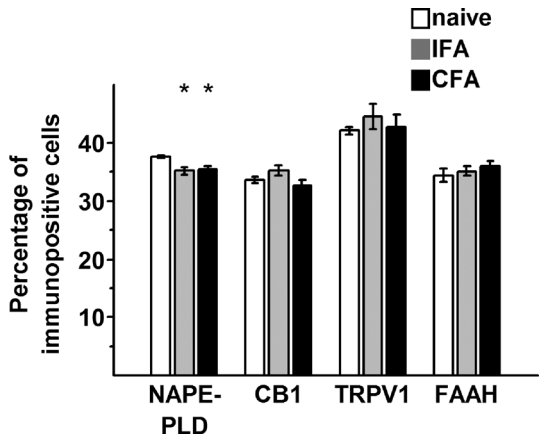

FIGURE 9 Both CFA and IFA injection into the hind paw reduce the number of NAPE-PLD-immunolabeled neurons without inducing any change in the number of TRPV1-, CB1 receptor-, or FAAH-immunolabeled neurons in DRG. Chart shows the relative number of neurons exhibiting immunopositivity for NAPE-PLD, CB1 receptor, TRPV1, and FAAH in naive (open bars), IFA-injected (gray bars), and CFA-injected (black bars) animals. Both IFA and CFA injection induced a small but significant reduction in the relative number of neurons exhibiting immunopositivity for NAPE-PLD. The number of immunopositive neurons for the other markers is not changed either by IFA or by CFA injection. Asterisks indicate significant differences from naive ($p = .01$ for IFA and $p = .02$ for CFA [$n = 3$ for both IFA and CFA], two-tailed Fisher's exact test). All data are expressed as mean ± SEM

Among the two major types of nociceptive primary sensory neurons, NAPE-PLD exhibits preference for IB4-binding cells. IB4-binding and peptidergic primary sensory neurons differ in their peripheral tissue targets, spinal projections, membrane protein expression, responses to painful events, and even in the brain areas where the information they convey is transmitted (Bennett, Averill, Clary, Priestley, & McMahon, 1996; Breese, George, Pauers, & Stucky, 2005; Perry & Lawson, 1998; Todd, 2010). Functionally, IB4-binding neurons are associated primarily with responses to noxious mechanical stimuli and the development of mechanical pain, although they may also contribute significantly to the development of thermal pain following nerve injury (Cavanaugh et al., 2009; Vilceanu, Honore, Hogan, & Stucky, 2010). Therefore, if NAPE-PLD is involved in nociceptive processing in primary sensory neurons, its activity could contribute to the regulation of mechanosensitivity and the development of mechanical pain.

Among the putative enzymatic pathways that are implicated in converting NAPE into N-acylethanolamine (NAEA), including anandamide (Liu et al., 2006, 2008; Okamoto et al., 2004; Simon & Cravatt, 2006, 2008), the NAPE-PLD-catalyzed pathway is the only one known to be Ca^{2+}-sensitive (Okamoto et al., 2004; Tsuboi et al., 2011; Ueda et al., 2001; Wang et al., 2006, 2008). van der Stelt and colleagues (2005) reported that increasing the intracellular Ca^{2+} concentration results in anandamide synthesis in cultured primary sensory neurons. These data indicate that NAPE-PLD is functional in cultured primary sensory neurons.

In addition to anandamide, related molecules, including palmitoylethanolamine (PEA) and oleoylethanolamine (OEA), are also synthesized by NAPE-PLD. Both PEA and OEA (and anandamide) activate the peroxisome proliferator-activated receptor-α (PPARα; Fu et al., 2003; Lo Verme et al., 2005; Sun, Alexander, Kendall, & Bennett, 2006) and the G protein-coupled receptor 119 (GPR119; Overton et al., 2006; Ryberg et al., 2007). Furthermore, PEA (and anandamide) also activates GPR55 (Lauckner et al., 2008; Ryberg et al., 2007). Although PPARα is expressed in both small- and large-diameter cells, GPR55 is expressed primarily in NF200-expressing large-diameter cells (Lauckner et al., 2008; Lo Verme et al., 2005). Therefore, the expression pattern of NAPE-PLD that we found in the present study suggests that NAPE-PLD, in addition to signaling through the CB1 receptor and TRPV1, could also be involved in signaling through PPARα and GPR55 in subpopulations of primary sensory neurons.

Consistent with the view that an autocrine signaling system that involves anandamide, the CB1 receptor, and TRPV1 could exist in a subpopulation of nociceptive primary sensory neurons (Sousa-Valente, Varga, Ananthan, Khajuria, & Nagy, 2014), we have shown here that

TABLE 2 Summary of the proportion of neurons expressing NAPE-PLD and other markers in L4–5 DRG from IFA-injected and CFA-injected animals[a]

		Number of cells used for analysis	Percentage of NAPE-PLD-expressing cells expressing various markers (*p* value)	Percentage of neurons expressing various markers together with NAPE-PLD (*p* value)
NAPE-PLD	IFA	3,872	35 ± 0.5 (.09)[b]	-
	CFA	4,181	35 ± 0.6 (.12)[b]	-
TRPV1	IFA	1,392	42 ± 0.2 (.92)[b]	54 ± 6.4 (.31)[b]
	CFA	1,625	43 ± 2.2 (.74)[b]	62 ± 1.6 (.67)[b]
CB1	IFA	1,006	35 ± 0.7 (.56)[b]	61 ± 1.0 (.40)[b]
	CFA	1,301	33 ± 0.9 (.66)[b]	65 ± 6.4 (.17)[b]
FAAH	IFA	1,474	35 ± 0.5 (.77)[b]	76 ± 9.0 (.16)[b]
	CFA	1,255	36 ± 0.8 (.52)[b]	69 ± 10.6 (.59)[b]

[a] $N = 3$ for each data point.
[b] Two-tailed Fisher exact test showing statistical differences at $p < .05$.

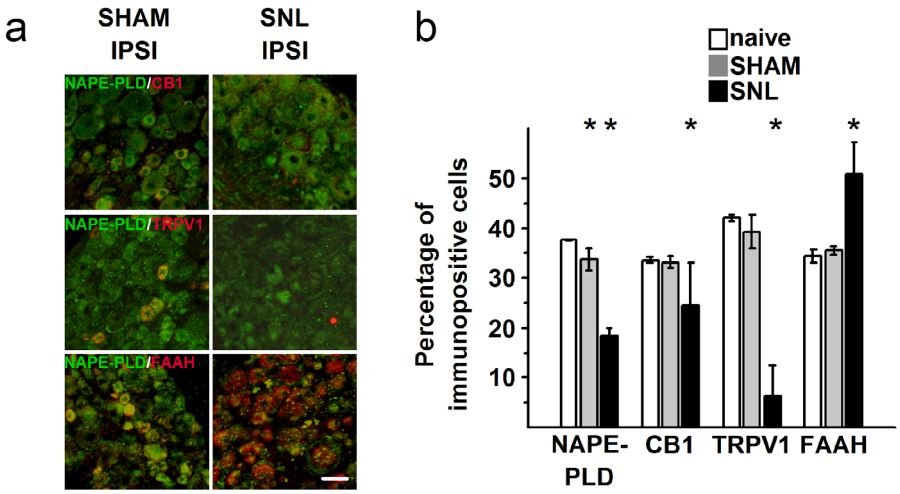

FIGURE 10 Ligation of the L5 spinal nerve induces reduction in the number of neurons exhibiting immunopositivity of NAPE-PLD, TRPV1, and the CB1 receptor, whereas it induces an increase in the number of neurons exhibiting immunopositivity of FAAH in the L5 DRG. (a) Typical images of DRG sections cut from the ipsilateral (IPSI) L5 DRG of a sham-operated rat (SHAM) and animals subjected to ligation of the L5 spinal nerve (SNL) and incubated in anti-NAPE-PLD, anti-CB1 receptor, anti-TRPV1, and anti-FAAH antibodies. The numbers of cells exhibiting immunopositivity for NAPE-PLD, the CB1 receptor, and TRPV1 were reduced following SNL, whereas the number of cells exhibiting immunopositivity for FAAH was increased following SNL. (b) Comparison among the number of primary sensory neurons exhibiting immunopositivity for NAPE-PLD, CB1 receptor, TRPV1, and FAAH in the ipsilateral L5 DRG of naïve rats (open bars), sham-operated rats (gray bars), and rats subjected to L5 SNL (black bars). SNL reduces the proportion of neurons expressing NAPE-PLD, TRPV1, and the CB1 receptor and increases the proportion of FAAH in the injured L5 DRG. ($p < .001$ for TRPV1, $p < .001$ for TRPV1, $p < .001$ for the CB1 receptor, and $p < 0.001$ for FAAH, two-tailed Fisher's exact test). In addition, the sham injury also reduced the number of neurons exhibiting immunopositivity for NAPE-PLD. Scale bar = 50 μm

NAPE-PLD exhibits a high degree of coexpression with both TRPV1 and the CB1 receptor. We have also demonstrated here that NAPE-PLD shows a high degree of coexpression with FAAH, which is expressed in the majority of TRPV1-expressing primary sensory neurons (Lever et al., 2009). Considering the coexpression patterns we found in the present study together with those published previously on TRPV1 and the CB1 receptor and on TRPV1 and FAAH coexpression (Agarwal et al., 2007; Ahluwalia et al., 2000; Binzen et al., 2006; Lever et al., 2009; Mitrirattanakul et al., 2006), it appears that the anatomical basis for an anandamide-, TRPV1-, CB1 receptor-, and FAAH-mediated autocrine signaling system indeed exists in the majority of nociceptive primary sensory neurons. Our recent finding that TRPV1 shows a high degree of coexpression with some of the enzymes implicated in Ca^{2+}-insensitive anandamide synthesis (Varga et al., 2014) suggests that anandamide could be synthesized both in Ca^{2+}-sensitive and in Ca^{2+}-insensitive manners in at least some of those primary sensory neurons.

Although TRPV1 activation by anandamide results in excitation (Ahluwalia et al., 2003; Potenzieri, Brink, & Simone, 2009; Zygmunt et al., 1999), CB1 receptor activation by this agent is generally considered as inhibitory in nociceptive primary sensory neurons (Calignano,

TABLE 3 Summary of the proportion of neurons expressing NAPE-PLD and other markers in Ipsilateral L5 DRG from sham operated and SNL Operated animals[a]

		Number of cells used for analysis	Percentage of NAPE-PLD-expressing cells expressing various markers (*p* value)	Percentage of neurons expressing various markers together with NAPE-PLD (*p* value)
NAPE-PLD	SHAM	1,932	34 ± 2.1 (.04)[b]	-
	SNL	1,962	19 ± 1.4 (.00)[b]	-
TRPV1	SHAM	668	39 ± 3.4 (.48)[b]	61 ± 8.8 (.60)[b]
	SNL	695	6 ± 6.2 (.00)[b]	5 ± 10.1 (.00)[b]
CB1	SHAM	614	33 ± 1.2 (.92)[b]	59 ± 6 (.04)[b]
	SNL	653	15 ± 1.8 (.00)[b]	49 ± 23.8 (.00)[b]
FAAH	SHAM	650	36 ± 2.8 (.71)[b]	63 ± 9.6 (1.00)[b]
	SNL	614	51 ± 6.5 (.00)[b]	83 ± 9.5 (.00)[b]

[a]$N = 3$ for each data point.
[b]Two-tailed Fisher exact test showing statistical differences at $p < .05$.

TABLE 4 Summary of the proportion of neurons expressing NAPE-PLD and other markers in ipsilateral L4 DRG from sham operated and SNL operated animals[a]

		Number of cells used for analysis	Percentage of NAPE-PLD-expressing cells expressing various markers (*p* value)	Percentage of neurons expressing various markers together with NAPE-PLD (*p* value)
NAPE-PLD	SHAM	1,907	36 ± 1.1 (.29)[b]	-
	SNL	1,982	38 ± 2.7 (.85)[b]	-
TRPV1	SHAM	631	41 ± 3.9 (.82)[b]	51 ± 8.8 (.11)[b]
	SNL	722	36 ± 6.3 (.12)[b]	56 ± 6.2 (.89)[b]
CB1	SHAM	679	33 ± 0.8 (.85)[b]	56 ± 14.9 (.02)[b]
	SNL	618	41 ± 1.0 (.03)[b]	71 ± 14.6 (.34)[b]
FAAH	SHAM	597	37 ± 0.3 (.37)[b]	66 ± 3.8 (.44)[b]
	SNL	642	38 ± 1.4 (.96)[b]	63 ± 10.7 (.89)[b]

[a]$N = 3$ for each data point.
[b]Two-tailed Fisher exact test showing statistical differences at $p < .05$.

La Rana, Giuffrida, & Piomelli, 1998; Chen et al., 2016; Clapper et al., 2010; Kelly, Jhaveri, Sagar, Kendall, & Chapman, 2003; Richardson, Kilo, & Hargreaves, 1998). The CB1 receptor-mediated inhibitory effect in those neurons results, inter alia, in the reduction of TRPV1-mediated responses (Binzen et al., 2006; Mahmud, Santha, Paule, & Nagy, 2009; Santha, Jenes, Somogyi, & Nagy, 2010). By hydrolyzing anandamide, FAAH could serve as a brake in both the anandamide-induced TRPV1- and CB1 receptor-mediated effects.

We recently showed that, although anandamide produced in a Ca^{2+}-insensitive fashion in cultured primary sensory neurons induces TRPV1-mediated excitation, it does not produce a CB1 receptor-mediated inhibitory effect when the inhibitory effect is assessed by measuring TRPV1-mediated responses (Varga et al., 2014). The finding that Ca^{2+}-sensitive anandamide production in primary sensory neurons results in TRPV1-mediated excitatory effects (van der Stelt et al., 2005) suggests that NAPE-PLD activity could also be associated with TRPV1 activation. However, although we found a strong correlation between NAPE-PLD- and CB1 receptor-immunostaining intensities, the correlation between NAPE-PLD- and TRPV1-immunostaining intensities is very low. These data suggest that, at least in intact DRG, NAPE-PLD activity may be linked to the CB1 receptor rather than to TRPV1 activation. If, indeed, anandamide produced in a Ca^{2+}-sensitive and a Ca^{2+}-insensitive manner has differing primary targets in primary sensory neurons, the anandamide-, CB1 receptor-, TRPV1-, and FAAH-formed putative autocrine signaling system could exert a very delicate control over the activity of a major proportion of nociceptive cells and, hence, over the development of pain. Consequently, any change in the expression or activity of any members of that system could disturb balanced signaling that may contribute to the development of pain.

Our data indicate that various types of painful disturbances of the homeostasis of peripheral tissues are able to produce such perturbation. Whereas CFA is used to induce a painful inflammatory reaction, IFA is used as its control, although IFA injection itself induces some inflammatory reaction and even hypersensitivity (Billiau & Matthys, 2001). Indeed, IFA injection induced a transient hypersensitivity in the present study. Furthermore, similarly to CFA injection, IFA also induced a small but nevertheless significant reduction in the number of NAPE-PLD-immunolabeled cells as well as in the high correlation of intensities between NAPE-PLD and CB1 receptor immunolabeling. Both IFA and CFA increased the ipsilateral/contralateral intensity ratio of TRPV1 immunolabeling (i.e., increased in intensity of TRPV1 immunolabeling on the ipsilateral side). The slight but significant reduction in the number of CB1 receptor-expressing cells produced by CFA and IFA is surprising because this is opposite to what had been previously reported (Amaya et al., 2006). Furthermore, the lack of increase in the number of TRPV1-expressing cells is also surprising because it differs from data that had been reported earlier (Amaya et al., 2004, 2006; Ji et al., 2002; Luo et al., 2004; Yu et al., 2008; but see Bar et al., 2004; Zhou et al., 2003). These differences could be due to the use of different analyzing techniques in the different studies. Nevertheless, the combined effects of the changes that we observed suggest that a balanced signaling between anandamide of NAPE-PLD origin and TRPV1 and the CB1 receptor is tipped toward a signaling with increased excitatory and reduced inhibitory components. However, the contribution of this unbalanced signaling could be negligible because, although the CFA injection-induced hypersensitivity is significantly greater than that produced by IFA injection, the changes in the expression pattern of the molecules are not.

A different type of perturbation of balanced endocannabinoid/endovanilloid signaling occurs following peripheral nerve injury because SNL reduces the number of NAPE-PLD- and CB1 receptor-expressing neurons, whereas it increases the number of FAAH-immunolabeled cells. These changes are expected to result in a dramatic reduction of inhibitory signaling between anandamide of NAPE-PLD origin and the CB1 receptor in the affected neurons. The nerve injury-induced downregulation of NAPE-PLD expression is consistent with a recent study showing that NAPE-PLD mRNA expression is reduced in the injury-affected DRG in another neuropathic pain model, the so-called spared nerve injury model (Bishay et al., 2010). Nerve injury-induced downregulation of NAPE-PLD expression is associated with a reduction in

NAEA content, including that of anandamide, of the affected DRG (Bishay et al., 2010, 2013; Mitrirattanakul et al., 2006). The nerve injury-induced upregulation of FAAH expression is also consistent with results from previous studies (Bishay et al., 2010), although, in our earlier study (Lever et al., 2009), the increase in the proportion of FAAH-expressing neurons did not reach the level of significance. This discrepancy between our present and previous data could be due to the transient nature of upregulation of FAAH expression, which reaches its peak on the seventh day after the injury (Bishay et al., 2010). Although we assessed nerve injury-induced changes 7 days after the surgery in both studies, because of possible slight differences in surgery techniques used by different persons, the time course of changes could be different. Nevertheless, the changes we found in CB1 receptor expression are generally consistent with previous reports (Costigan et al., 2002; Mitrirattanakul et al., 2006; Zhang et al., 2007). Finally, in addition to changes in the proportions of NAPE-PLD-, CB1 receptor-, and FAAH-expressing neurons, the proportion of TRPV1-expressing DRG neurons is also dramatically reduced by SNL. This change is similar to that reported earlier by others who used the same neuropathic model (Hudson et al., 2001; Lever et al., 2009). This reduced TRPV1 expression is consistent with the limited role of this ion channel in the development of pain following peripheral nerve injury (Caterina et al., 2000).

In summary, this study shows that a major proportion of primary sensory neurons express NAPE-PLD. We also show that NAPE-PLD exhibits a high degree of coexpression with TRPV1, the CB1 receptor, and FAAH, indicating that NAPE-PLD indeed could be involved in an autocrine regulatory mechanism in a major proportion of nociceptive primary sensory neurons. Finally, we show that, although peripheral inflammation and injury to peripheral nerves induce differing changes in the expression pattern of NAPE-PLD, the CB1 receptor, TRPV1, and FAAH, both sets of changes are highly likely to produce unbalanced signaling in that autocrine regulatory system and that unbalanced signaling is characterized primarily by reduced anandamide-induced and CB1 receptor-mediated activity and, hence, reduced inhibition on the activity and excitability of primary sensory neurons. Similar unbalanced endocannabinoid/endovanilloid signaling because of reduction in CB1 receptor-mediated inhibitory effects in primary sensory neurons as well as in the spinal cord has been shown to contribute to the development of pain in various animal models of persistent pain (Bishay et al., 2010; Guasti et al., 2009; Jhaveri, Richardson, Kendall, Barrett, & Chapman, 2006; Khasabova et al., 2008, 2012, 2013; Starowicz & Przewlocka, 2012; Starowicz et al., 2012, 2013).

The findings we present here provide the first insight into an autocrine signaling system that is highly likely to play an important role in regulating the excitability of a major group of nociceptive primary sensory neurons. This insight is important because it suggests that pharmacological manipulation of this system might provide a significant reduction in spinal nociceptive input and, hence, reduction in pain associated with peripheral pathologies. However, full utilization of the putative analgesic potential of this system requires further elucidation of the signaling mechanism. For example, we recently showed that spatial proximity and protein–protein interactions between TRPV1 and the CB1 receptor may determine how the CB1 receptor affects TRPV1 activity (Chen et al., 2016). Similarly, the spatial relationship between FAAH and TRPV1 and/or the CB1 receptor, which is currently unknown, is of high importance because it determines whether FAAH activity directs anandamide away from the CB1 receptor or TRPV1. Furthermore, although our data suggest that anandamide synthesized by NAPE-PLD may preferentially activate the CB1 receptor, this assumption requires further support.

It is also important to note that, to avoid inducing undesirable effects, manipulation of the endocannabinoid/endovanilloid autocrine signaling system even outside the blood–brain barrier should occur in a cell-specific manner (i.e., in nociceptive primary sensory neurons) because several components of the endocannabinoid/endovanilloid system exhibit widespread expression patterns. Therefore, although the CB1 receptor and TRPV1 outside the central nervous system are expressed almost exclusively by nociceptive primary sensory neurons (Agarwal et al., 2007; Ahluwalia et al., 2000; Binzen et al., 2006; Caterina et al., 1997; Mitrirattanakul et al., 2006; Sousa-Valente, Andreou, et al., 2014; Tominaga et al., 1998; Veress et al., 2013), both NAPE-PLD and FAAH are expressed by various cells and are involved in various physiological functions (Alhouayek & Muccioli, 2012; Geurts et al., 2015; Guo et al., 2005; Paria, Zhao, Wang, Das, & Dey, 1999; Rossi et al., 2009). Nevertheless, our data indicate that NAPE-PLD could be another important molecule of the endocannabinoid/endovanilloid system that controls nociceptive processing in primary sensory neurons. Therefore, we propose that NAPE-PLD in nociceptive primary sensory neurons could be a valuable novel target for the development of new analgesics.

CONFLICT OF INTEREST

The authors have no conflicts of interest associated with this work.

AUTHOR CONTRIBUTIONS

JS-V: majority of immunolabeling and data analysis, behavioral experiments, drafting of the manuscript. AV: immunolabeling, Western blotting, PCR, drafting of the manuscript. JVTP: in situ hybridization, immunolabeling. AJ: immunolabeling, statistical analysis, drafting of the manuscript. JW: PCR. KM: drafting of the manuscript, finalizing the article. BC: FAAH antibody, finalizing the article. NU: NAPE-PLD$^{-/-}$ mice, finalizing article. KT: NAPE-PLD$^{-/-}$ mice, finalizing the article. PS: imaging, statistics, drafting of the manuscript. GJ: imaging, statistics, drafting of the manuscript. HT: immunolabeling. AA: project management, drafting of the manuscript. IN: project management, drafting of the manuscript.

DATA ACCESSIBILITY

Aviva Systems Biology catalog No. ARP55927_P050, RRID: AB_2046809; Abcam catalog No. AB22569, RRID:AB_725809; Cravatt's Laboratory, RRID:AB_2314388.

REFERENCES

Agarwal, N., Pacher, P., Tegeder, I., Amaya, F., Constantin, C. E., Brenner, G. J ... Kuner, R. (2007). Cannabinoids mediate analgesia largely via peripheral type 1 cannabinoid receptors in nociceptors. *Nature Neuroscience*, *10*, 870–879.

Ahluwalia, J., Urban, L., Bevan, S., & Nagy, I. (2003). Anandamide regulates neuropeptide release from capsaicin-sensitive primary sensory neurons by activating both the cannabinoid 1 receptor and the vanilloid receptor 1 in vitro. *Eur J Neurosci*, *17*, 2611–2618.

Ahluwalia, J., Urban, L., Capogna, M., Bevan, S., & Nagy, I. (2000). Cannabinoid 1 receptors are expressed in nociceptive primary sensory neurons. *Neuroscience*, *100*, 685–688.

Alhouayek, M., & Muccioli, G. G. (2012). The endocannabinoid system in inflammatory bowel diseases: From pathophysiology to therapeutic opportunity. *Trends Mol Med*, *18*, 615–625.

Amaya, F., Shimosato, G., Kawasaki, Y., Hashimoto, S., Tanaka, Y., Ji, R. R., & Tanaka, M. (2006). Induction of CB1 cannabinoid receptor by inflammation in primary afferent neurons facilitates antihyperalgesic effect of peripheral CB1 agonist. *Pain*, *124*, 175–183.

Amaya, F., Shimosato, G., Nagano, M., Ueda, M., Hashimoto, S., Tanaka, Y., ... Tanaka, M. (2004). NGF and GDNF differentially regulate TRPV1 expression that contributes to development of inflammatory thermal hyperalgesia. *Eur J Neurosci*, *20*, 2303–2310.

Bar, K. J., Schaible, H. G., Brauer, R., Halbhuber, K. J., & von Banchet, G. S. (2004). The proportion of TRPV1 protein-positive lumbar DRG neurones does not increase in the course of acute and chronic antigen-induced arthritis in the knee joint of the rat. *Neurosci Lett*, *361*, 172–175.

Bennett, D. L., Averill, S., Clary, D. O., Priestley, J. V., & McMahon, S. B. (1996). Postnatal changes in the expression of the TrkA high-affinity NGF receptor in primary sensory neurons. *Eur J Neurosci*, *8*, 2204–2208.

Billiau, A., & Matthys, P. (2001). Modes of action of Freund's adjuvants in experimental models of autoimmune diseases. *J Leukoc Biol*, *70*, 849–860.

Binzen, U., Greffrath, W., Hennessy, S., Bausen, M., Saaler-Reinhardt, S., & Treede, R. D. (2006). Coexpression of the voltage-gated potassium channel Kv1.4 with transient receptor potential channels (TRPV1 and TRPV2) and the cannabinoid receptor CB1 in rat dorsal root ganglion neurons. *Neuroscience*, *142*, 527–539.

Bishay, P., Haussler, A., Lim, H. Y., Oertel, B., Galve-Roperh, I., Ferreiros, N., & Tegeder, I. (2013). Anandamide deficiency and heightened neuropathic pain in aged mice. *Neuropharmacology*, *71*, 204–215.

Bishay, P., Schmidt, H., Marian, C., Haussler, A., Wijnvoord, N., Ziebell, S., ... Tegeder, I. (2010). R-flurbiprofen reduces neuropathic pain in rodents by restoring endogenous cannabinoids. *PLoS One*, *5*(5), e10628.

Breese, N. M., George, A. C., Pauers, L. E., & Stucky, C. L. (2005). Peripheral inflammation selectively increases TRPV1 function in IB4-positive sensory neurons from adult mouse. *Pain*, *115*, 37–49.

Calignano, A., La Rana, G., Giuffrida, A., & Piomelli, D. (1998). Control of pain initiation by endogenous cannabinoids. *Nature*, *394*, 277–281.

Caterina, M. J., Leffler, A., Malmberg, A. B., Martin, W. J., Trafton, J., Petersen-Zeitz, K. R., ... Julius, D. (2000). Impaired nociception and pain sensation in mice lacking the capsaicin receptor. *Science*, *288*, 306–313.

Caterina, M. J., Schumacher, M. A., Tominaga, M., Rosen, T. A., Levine, J. D., & Julius, D. (1997). The capsaicin receptor: A heat-activated ion channel in the pain pathway. *Nature*, *389*, 816–824.

Cavanaugh, D. J., Lee, H., Lo, L., Shields, S. D., Zylka, M. J., Basbaum, A. I., & Anderson, D. J. (2009). Distinct subsets of unmyelinated primary sensory fibers mediate behavioral responses to noxious thermal and mechanical stimuli. *Proc Natl Acad Sci U S A*, *106*, 9075–9080.

Chen, J., Varga, A., Selvarajah, S., Jenes, A., Dienes, B., Sousa-Valente, J., ... Nagy, I. (2016). Spatial distribution of the cannabinoid type 1 and capsaicin receptors may contribute to the complexity of their cross-talk. *Scientific Reports*, *6*, 33307.

Clapper, J. R., Moreno-Sanz, G., Russo, R., Guijarro, A., Vacondio, F., Duranti, A., ... Piomelli, D. (2010). Anandamide suppresses pain initiation through a peripheral endocannabinoid mechanism. *Nat Neurosci*, *13*, 1265–1270.

Costigan, M., Befort, K., Karchewski, L., Griffin, R. S., D'Urso, D., Allchorne, A., ... Woolf, C. J. (2002). Replicate high-density rat genome oligonucleotide microarrays reveal hundreds of regulated genes in the dorsal root ganglion after peripheral nerve injury. *BMC Neuroscience*, *3*, 16.

Cravatt, B. F., Giang, D. K., Mayfield, S. P., Boger, D. L., Lerner, R. A., & Gilula, N. B. (1996). Molecular characterization of an enzyme that degrades neuromodulatory fatty-acid amides. *Nature*, *384*, 83–87.

Cruz, C. D., Charrua, A., Vieira, E., Valente, J., Avelino, A., & Cruz, F. (2008). Intrathecal delivery of resiniferatoxin (RTX) reduces detrusor overactivity and spinal expression of TRPV1 in spinal cord injured animals. *Exp Neurol*, *214*, 301–308.

Devane, W. A., Hanus, L., Breuer, A., Pertwee, R. G., Stevenson, L. A., Griffin, G., ... Mechoulam, R. (1992). Isolation and structure of a brain constituent that binds to the cannabinoid receptor. *Science*, *258*, 1946–1949.

Fu, J., Gaetani, S., Oveisi, F., Lo Verme, J., Serrano, A., Rodriguez De Fonseca, F., ... Piomelli, D. (2003). Oleylethanolamide regulates feeding and body weight through activation of the nuclear receptor PPAR-alpha. *Nature*, *425*, 90–93.

Geurts, L., Everard, A., Van Hul, M., Essaghir, A., Duparc, T., Matamoros, S., ... Cani, P. D. (2015). Adipose tissue NAPE-PLD controls fat mass development by altering the browning process and gut microbiota. *Nat Commun*, *6*, 6495.

Guasti, L., Richardson, D., Jhaveri, M., Eldeeb, K., Barrett, D., Elphick, M. R., ... Chapman, V. (2009). Minocycline treatment inhibits microglial activation and alters spinal levels of endocannabinoids in a rat model of neuropathic pain. *Mol Pain*, *5*, 35.

Guo, Y., Wang, H., Okamoto, Y., Ueda, N., Kingsley, P. J., Marnett, L. J., ... Dey, S. K. (2005). N-acylphosphatidylethanolamine-hydrolyzing phospholipase D is an important determinant of uterine anandamide levels during implantation. *J Biol Chem*, *280*, 23429–23432.

Hammond, D. L., Ackerman, L., Holdsworth, R., & Elzey, B. (2004). Effects of spinal nerve ligation on immunohistochemically identified neurons in the L4 and L5 dorsal root ganglia of the rat. *J Comp Neurol*, *475*, 575–589.

Hargreaves, K., Dubner, R., Brown, F., Flores, C., & Joris, J. (1988). A new and sensitive method for measuring thermal nociception in cutaneous hyperalgesia. *Pain*, *32*, 77–88.

Hudson, L. J., Bevan, S., Wotherspoon, G., Gentry, C., Fox, A., & Winter, J. (2001). VR1 protein expression increases in undamaged DRG neurons after partial nerve injury. *Eur J Neurosci*, *13*, 2105–2114.

Jhaveri, M. D., Richardson, D., Kendall, D. A., Barrett, D. A., & Chapman, V. (2006). Analgesic effects of fatty acid amide hydrolase inhibition in a rat model of neuropathic pain. *J Neurosci*, *26*, 13318–13327.

Ji, R. R., Samad, T. A., Jin, S. X., Schmoll, R., & Woolf, C. J. (2002). p38 MAPK activation by NGF in primary sensory neurons after inflammation increases TRPV1 levels and maintains heat hyperalgesia. *Neuron*, *36*, 57–68.

Kelly, S., Jhaveri, M. D., Sagar, D. R., Kendall, D. A., & Chapman, V. (2003). Activation of peripheral cannabinoid CB1 receptors inhibits mechanically evoked responses of spinal neurons in noninflamed rats and rats with hindpaw inflammation. *Eur J Neurosci*, *18*, 2239–2243.

Khasabova, I. A., Holman, M., Morse, T., Burlakova, N., Coicou, L., Harding-Rose, C., ... Seybold, V. S. (2013). Increased anandamide uptake by sensory neurons contributes to hyperalgesia in a model of cancer pain. *Neurobiol Dis*, *58*, 19–28.

Khasabova, I. A., Khasabov, S. G., Harding-Rose, C., Coicou, L. G., Seybold, B. A., Lindberg, A. E., ... Seybold, V. S. (2008). A decrease in anandamide signaling contributes to the maintenance of cutaneous mechanical hyperalgesia in a model of bone cancer pain. *J Neurosci*, *28*, 11141–11152.

Khasabova, I. A., Khasabov, S., Paz, J., Harding-Rose, C., Simone, D. A., & Seybold, V. S. (2012). Cannabinoid type-1 receptor reduces pain and neurotoxicity produced by chemotherapy. *J Neurosci*, *32*, 7091–7101.

Kim, S. H., & Chung, J. M. (1992). An experimental model for peripheral neuropathy produced by segmental spinal nerve ligation in the rat. *Pain*, *50*, 355–363.

Lauckner, J. E., Jensen, J. B., Chen, H. Y., Lu, H. C., Hille, B., & Mackie, K. (2008). GPR55 is a cannabinoid receptor that increases intracellular calcium and inhibits M current. *Proc Natl Acad Sci U S A*, *105*, 2699–2704.

Lawson, S. N., Harper, A. A., Harper, E. I., Garson, J. A., & Anderton, B. H. (1984). A monoclonal antibody against neurofilament protein specifically labels a subpopulation of rat sensory neurones. *J Comp Neurol*, *228*, 263–272.

Lawson, S. N., & Waddell, P. J. (1991). Soma neurofilament immunoreactivity is related to cell-size and fiber conduction-velocity in rat primary sensory neurons. *J Physiol*, *435*, 41–63.

Leung, D., Saghatelian, A., Simon, G. M., & Cravatt, B. F. (2006). Inactivation of N-acyl phosphatidylethanolamine phospholipase D reveals multiple mechanisms for the biosynthesis of endocannabinoids. *Biochemistry*, *45*, 4720–4726.

Lever, I. J., Robinson, M., Cibelli, M., Paule, C., Santha, P., Yee, L., ... Rice, A. S. (2009). Localization of the endocannabinoid-degrading enzyme fatty acid amide hydrolase in rat dorsal root ganglion cells and its regulation after peripheral nerve injury. *J Neurosci*, *29*, 3766–3780.

Liu, J., Wang, L., Harvey-White, J., Huang, B. X., Kim, H. Y., Luquet, S., ... Kunos, G. (2008). Multiple pathways involved in the biosynthesis of anandamide. *Neuropharmacology*, *54*, 1–7.

Liu, J., Wang, L., Harvey-White, J., Osei-Hyiaman, D., Razdan, R., Gong, Q., ... Kunos, G. (2006). A biosynthetic pathway for anandamide. *Proc Natl Acad Sci U S A*, *103*, 13345–13350.

Lo Verme, J., Fu, J., Astarita, G., La Rana, G., Russo, R., Calignano, A., & Piomelli, D. (2005). The nuclear receptor peroxisome proliferator-activated receptor-alpha mediates the anti-inflammatory actions of palmitoylethanolamide. *Mol Pharmacol*, *67*, 15–19.

Luo, H., Cheng, J., Han, J. S., & Wan, Y. (2004). Change of vanilloid receptor 1 expression in dorsal root ganglion and spinal dorsal horn during inflammatory nociception induced by complete Freund's adjuvant in rats. *Neuroreport*, *15*, 655–658.

Mackie, K., & Hille, B. (1992). Cannabinoids inhibit N-type calcium channels in neuroblastoma-glioma cells. *Proc Natl Acad Sci U S A*, *89*, 3825–3829.

Mackie, K., Lai, Y., Westenbroek, R., & Mitchell, R. (1995). Cannabinoids activate an inwardly rectifying potassium conductance and inhibit Q-type calcium currents in AtT20 cells transfected with rat brain cannabinoid receptor. *J Neurosci*, *15*, 6552–6561.

Mahmud, A., Santha, P., Paule, C. C., & Nagy, I. (2009). Cannabinoid 1 receptor activation inhibits transient receptor potential vanilloid type 1 receptor-mediated cationic influx into rat cultured primary sensory neurons. *Neuroscience*, *162*, 1202–1211.

Malek, N., Mrugala, M., Makuch, W., Kolosowska, N., Przewlocka, B., Binkowski, M., ... Starowicz, K. (2015). A multitarget approach for pain treatment, dual inhibition of fatty acid amide hydrolase and TRPV1 in a rat model of osteoarthritis. *Pain*, *156*, 890–903.

Matsuda, L. A., Lolait, S. J., Brownstein, M. J., Young, A. C., & Bonner, T. I. (1990). Structure of a cannabinoid receptor and functional expression of the cloned cDNA. *Nature*, *346*, 561–564.

Michael, G. J., & Priestley, J. V. (1999). Differential expression of the mRNA for the vanilloid receptor subtype 1 in cells of the adult rat dorsal root and nodose ganglia and its downregulation by axotomy. *J Neurosci*, *19*, 1844–1854.

Mitrirattanakul, S., Ramakul, N., Guerrero, A. V., Matsuka, Y., Ono, T., Iwase, H., ... Spigelman, I. (2006). Site-specific increases in peripheral cannabinoid receptors and their endogenous ligands in a model of neuropathic pain. *Pain*, *126*, 102–114.

Nagy, B., Fedonidis, C., Photiou, A., Wahba, J., Paule, C. C., Ma, D., ... Nagy, I. (2009). Capsaicin-sensitive primary sensory neurons in the mouse express N-Acyl phosphatidylethanolamine phospholipase D. *Neuroscience*, *161*, 572–577.

Nagy, I., Friston, D., Valente, J. S., Perez, J. V. T., & Andreou, A. P. (2014). Pharmacology of the capsaicin receptor, transient receptor potential vanilloid type-1 ion channel. *Prog Drug Res*, *68*, 39–76.

Nagy, I., Santha, P., Jancso, G., & Urban, L. (2004). The role of the vanilloid (capsaicin) receptor (TRPV1) in physiology and pathology. *Eur J Pharmacol*, *500*, 351–369.

Okamoto, Y., Morishita, J., Tsuboi, K., Tonai, T., & Ueda, N. (2004). Molecular characterization of a phospholipase D generating anandamide and its congeners. *J Biol Chem*, *279*, 5298–5305.

Overton, H. A., Babbs, A. J., Doel, S. M., Fyfe, M. C., Gardner, L. S., Griffin, G., ... Reynet, C. (2006). Deorphanization of a G protein-coupled receptor for oleoylethanolamide and its use in the discovery of small-molecule hypophagic agents. *Cell Metab*, *3*, 167–175.

Paria, B. C., Zhao, X., Wang, J., Das, S. K., & Dey, S. K. (1999). Fatty-acid amide hydrolase is expressed in the mouse uterus and embryo during the peri-implantation period. *Biol Reprod*, *60*, 1151–1157.

Perry, M. J., & Lawson, S. N. (1998). Differences in expression of oligosaccharides, neuropeptides, carbonic anhydrase, and neurofilament in rat primary afferent neurons retrogradely labeled via skin, muscle, or visceral nerves. *Neuroscience*, *85*, 293–310.

Potenzieri, C., Brink, T. S., & Simone, D. A. (2009). Excitation of cutaneous C nociceptors by intraplantar administration of anandamide. *Brain Res*, *1268*, 38–47.

Richardson, J. D., Kilo, S., & Hargreaves, K. M. (1998). Cannabinoids reduce hyperalgesia and inflammation via interaction with peripheral CB1 receptors. *Pain*, *75*, 111–119.

Rossi, F., Siniscalco, D., Luongo, L., De Petrocellis, L., Bellini, G., Petrosino, S., ... Maione, S. (2009). The endovanilloid/endocannabinoid system in human osteoclasts: possible involvement in bone formation and resorption. *Bone*, *44*, 476–484.

Ryberg, E., Larsson, N., Sjogren, S., Hjorth, S., Hermansson, N. O., Leonova, J., ... Greasley, P. J. (2007). The orphan receptor GPR55 is a novel cannabinoid receptor. *Br J Pharmacol*, *152*, 1092–1101.

Santha, P., Jenes, A., Somogyi, C., & Nagy, I. (2010). The endogenous cannabinoid anandamide inhibits transient receptor potential vanilloid type 1 receptor-mediated currents in rat cultured primary sensory neurons. *Acta Physiol Hung*, *97*, 149–158.

Silverman, J. D., & Kruger, L. (1990). Selective neuronal glycoconjugate expression in sensory and autonomic ganglia: Relation of lectin reactivity to peptide and enzyme markers. *J Neurocytol*, *19*, 789–801.

Simon, G. M., & Cravatt, B. F. (2006). Endocannabinoid biosynthesis proceeding through glycerophospho-N-acyl ethanolamine and a role for alpha/beta-hydrolase 4 in this pathway. *J Biol Chem*, *281*, 26465–26472.

Simon, G. M., & Cravatt, B. F. (2008). Anandamide biosynthesis catalyzed by the phosphodiesterase GDE1 and detection of glycerophospho-N-acyl ethanolamine precursors in mouse brain. *J Biol Chem*, *283*, 9341–9349.

Sousa-Valente, J., Andreou, A. P., Urban, L., & Nagy, I. (2014). Transient receptor potential ion channels in primary sensory neurons as targets for novel analgesics. *Br J Pharmacol*, *171*, 2508–2527.

Sousa-Valente, J., Varga, A., Ananthan, K., Khajuria, A., & Nagy, I. (2014). Anandamide in primary sensory neurons: Too much of a good thing? *Eur J Neurosci*, *39*, 409–418.

Starowicz, K., Makuch, W., Korostynski, M., Malek, N., Slezak, M., Zychowska, M., … Di Marzo, V. (2013). Full inhibition of spinal FAAH leads to TRPV1-mediated analgesic effects in neuropathic rats and possible lipoxygenase-mediated remodeling of anandamide metabolism. *PLoS One*, *8*(4), e60040.

Starowicz, K., Makuch, W., Osikowicz, M., Piscitelli, F., Petrosino, S., Di Marzo, V., & Przewlocka, B. (2012). Spinal anandamide produces analgesia in neuropathic rats: Possible CB(1)- and TRPV1-mediated mechanisms. *Neuropharmacology*, *62*, 1746–1755.

Starowicz, K., & Przewlocka, B. (2012). Modulation of neuropathic pain-related behavior by the spinal endocannabinoid/endovanilloid system. *Philos Trans R Soc Lond B Biol Sci*, *367*, 3286–3299.

Suarez, J., Bermudez-Silva, F. J., Mackie, K., Ledent, C., Zimmer, A., Cravatt, B. F., & de Fonseca, F. R. (2008). Immunohistochemical description of the endogenous cannabinoid system in the rat cerebellum and functionally related nuclei. *J Comp Neurol*, *509*, 400–421.

Sun, Y., Alexander, S. P., Kendall, D. A., & Bennett, A. J. (2006). Cannabinoids and PPARalpha signalling. *Biochem Soc Trans*, *34*, 1095–1097.

Todd, A. J. (2010). Neuronal circuitry for pain processing in the dorsal horn. *Nat Rev Neurosci*, *11*, 823–836.

Tominaga, M., Caterina, M. J., Malmberg, A. B., Rosen, T. A., Gilbert, H., Skinner, K., … Julius, D. (1998). The cloned capsaicin receptor integrates multiple pain-producing stimuli. *Neuron*, *21*, 531–543.

Tsuboi, K., Okamoto, Y., Ikematsu, N., Inoue, M., Shimizu, Y., Uyama, T., … Ueda, N. (2011). Enzymatic formation of N-acylethanolamines from N-acylethanolamine plasmalogen through N-acylphosphatidylethanolamine-hydrolyzing phospholipase D-dependent and -independent pathways. *Biochim Biophys Acta*, *1811*, 565–577.

Twitchell, W., Brown, S., & Mackie, K. (1997). Cannabinoids inhibit N- and P/Q-type calcium channels in cultured rat hippocampal neurons. *J Neurophysiol*, *78*, 43–50.

Ueda, N., Liu, Q., & Yamanaka, K. (2001). Marked activation of the N-acylphosphatidylethanolamine-hydrolyzing phosphodiesterase by divalent cations. *Biochim Biophys Acta*, *1532*, 121–127.

Valente, J., Tailor, H., Jenes, A., Mackie, K., Cravatt, B. F., Buluwala, L., … Nagy, I. (2011). Expression of N-acyl phosphotidylethanolamine phospholipase D in rat dorsal root ganglion neurons. *Proc Phys Soc*, *22*, PC25.

van der Stelt, M., & Di Marzo, V. (2005). Anandamide as an intracellular messenger regulating ion channel activity. *Prostaglandins Other Lipid Mediat*, *77*, 111–122.

van der Stelt, M., Trevisani, M., Vellani, V., De Petrocellis, L., Schiano Moriello, A., Campi, B., … Di Marzo, V. (2005). Anandamide acts as an intracellular messenger amplifying Ca^{2+} influx via TRPV1 channels. *EMBO J*, *24*, 3026–3037.

Varga, A., Jenes, A., Marczylo, T. H., Sousa-Valente,. J, Chen, J., Austin, J., … Nagy, I. (2014). Anandamide produced by Ca^{2+}-insensitive enzymes induces excitation in primary sensory neurons. *Pflugers Arch*, *466*, 1421–1435.

Vellani, V., Petrosino, S., De Petrocellis, L., Valenti, M., Prandini, M., Magherini, P. C., … Di Marzo, V. (2008). Functional lipidomics. Calcium-independent activation of endocannabinoid/endovanilloid lipid signaling in sensory neurons by protein kinases C and A and thrombin. *Neuropharmacology*, *55*, 1274–1279.

Veress, G., Meszar, Z., Muszil, D., Avelino, A., Matesz, K., Mackie, K., & Nagy, I. (2013). Characterisation of cannabinoid 1 receptor expression in the perikarya and peripheral and spinal processes of primary sensory neurons. *Brain Struct Funct*, *218*, 733–750.

Vilceanu, D., Honore, P., Hogan, Q. H., & Stucky, C. L. (2010). Spinal nerve ligation in mouse upregulates TRPV1 heat function in injured IB4-positive nociceptors. *J Pain*, *11*, 588–599.

Wang, J., Okamoto, Y., Morishita, J., Tsuboi, K., Miyatake, A., & Ueda, N. (2006). Functional analysis of the purified anandamide-generating phospholipase D as a member of the metallo-beta-lactamase family. *J Biol Chem*, *281*, 12325–12335.

Wang, J., Okamoto, Y., Tsuboi, K., & Ueda, N. (2008). The stimulatory effect of phosphatidylethanolamine on N-acylphosphatidylethanolamine-hydrolyzing phospholipase D (NAPE-PLD). *Neuropharmacology*, *54*, 8–15.

White, J. P., Urban, L., & Nagy, I. (2011). TRPV1 function in health and disease. *Curr Pharm Biotechnol*, *12*, 130–144.

Yu, L., Yang, F., Luo, H., Liu, F. Y., Han, J. S., Xing, G. G., & Wan, Y. (2008). The role of TRPV1 in different subtypes of dorsal root ganglion neurons in rat chronic inflammatory nociception induced by complete Freund's adjuvant. *Mol Pain*, *4*, 61.

Zhang, S., Zhao, B., Jiang, H., Wang, B., & Ma, B. (2007). Cationic lipids and polymers mediated vectors for delivery of siRNA. *J Control Release*, *123*, 1–10.

Zhou, Y., Li, G. D., & Zhao, Z. Q. (2003). State-dependent phosphorylation of epsilon-isozyme of protein kinase C in adult rat dorsal root ganglia after inflammation and nerve injury. *J Neurochem*, *85*, 571–580.

Zimmerman, M. (1983). Ethical guidelines for investigations of experimental pain in conscious animals. *Pain*, *16*, 109–110.

Zygmunt, P. M., Petersson, J., Andersson, D. A., Chuang, H., Sorgard, M., Di Marzo, V., … Hogestatt, E. D. (1999). Vanilloid receptors on sensory nerves mediate the vasodilator action of anandamide. *Nature*, *400*, 452–457.

How to cite this article: Sousa-Valente J, Varga V, Perez JVT, Jenes A, Wahba J, Mackie K, Cravatt B, Ueda N, Tsuboi K, Santha P, Jancso G, Tailor H, Avelino A, Nagy I. Inflammation of peripheral tissues and injury to peripheral nerves induce differing effects in the expression of the calcium-sensitive N-arachydonoylethanolamine-synthesizing enzyme and related molecules in rat primary sensory neurons. *J. Comp. Neurol.* 2017;525:1778–1796. https://doi.org/10.1002/cne.24154